Advances in Aircraft and Spacecraft Science, *Vol. 11, No. 3 (2024) 269-297*
https://doi.org/10.12989/aas.2024.11.3.269

Electromechanical bending of Porous Functionally Graded Piezoelectric (PFGP) nanobeams with flexoelectricity

Alaa A. Abdelrahman[1], Hanaa E. Abdel-Mottaleb[2], Mohamed A. Eltaher*[3], Azza M. Abdraboh[4] and Abdallah M. Kabeel[1]

[1]*Mechanical Design & Production Department, Faculty of Engineering, Zagazig University, P.O. Box 44519, Zagazig, Egypt*
[2]*Structural Engineering Department, Faculty of Engineering, Zagazig University, P.O. Box 44519, Zagazig, Egypt*
[3]*Mechanical Engineering Department, Faculty of Engineering, King Abdulaziz University, P.O. Box 80204, Jeddah, Saudi Arabia*
[4]*Physics Department, Faculty of Science, Benha University, Benha, Egypt*

(Received October 6, 2023, Revised December 4, 2024, Accepted December 10, 2024)

Abstract. This study develops a size-dependent model based on modified nonlocal strain gradient theory to examine the effects of flexoelectricity and porosity distribution on the electromechanical bending behavior of piezoelectric functionally graded (FG) nanocomposite beams on Winkler-Pasternak foundations under different loading conditions. The nanocomposite comprises a porous FG core with piezoelectric face layers, using a nonlinear power law for thorough-thickness FG material gradation. Various porosity distribution patterns are considered, and closed-form solutions for electromechanical bending deflection are derived and validated. Results show that nonclassical bending behavior can be optimized by adjusting FG gradation, porosity, flexoelectricity, and foundation parameters, providing insights for MEMS and NEMS applications.

Keywords: electromechanical bending; flexoelectric; functionally graded porous material; modified electromechanical nonlocal strain gradient theory; piezoelectric layers; porosity distribution; Winkler-Pasternak elastic foundation

1. Introduction

In recent years, piezoelectric materials and smart structures have garnered significant attention due to their ability to convert mechanical energy into electrical energy and vice versa. This electromechanical coupling mechanism has enabled their widespread application in various engineering and technological fields, including sensors, actuators, and energy harvesters, (Zhang *et al*. 2022, Zheng *et al*. 2023, Alessi *et al*. 2023, Abdelrahman *et al*. 2023b). To further enhance the performance of these structural systems and devices, researchers have explored the integration of functionally graded materials, (Zhao *et al*. 2020, 2022, Alnujaie *et al*. 2023, Zheng *et al*. 2024). To effectively capture the mechanical performance of piezoelectric nanostructural systems, advanced continuum theories, such as nonlocal elasticity, strain gradient theory, and surface elasticity

*Corresponding author, Ph.D., E-mail: meltaher@kau.edu.sa, mohaeltaher@gmail.com

http://www.techno-press.org/?journal=aas&subpage=7 ISSN: 2287-528X (Print), 2287-5271 (Online)

theory, have been employed. These nonclassical approaches account for size-dependent influences that become increasingly important at the nanoscale. By incorporating these theories into the analysis of piezoelectric nanostructural systems, researchers can design and optimize devices with enhanced performance and functionality, (Selvamani *et al*. 2022, Abdelrahman *et al*. 2023c, Abdelrahman *et al*. 2024a).

Microelectromechanical and nanoelectromechanical systems, (MEMS) & (NEMS) have garnered significant research interest due to their promising features, such as small size, low power consumption, high reliability, and precision. The performance of MEMS and NEMS are significantly dependent on material characteristics and actuation mechanisms, Zhao *et al*. (2023). Functionally graded materials (FGMs), a class of advanced modern composite materials with continuously varying material properties, offer several promising advantages for MEMS and NEMS applications, including improved temperature tolerance, fracture toughness, and stress intensity factor, (Dang and Do 2021, Melaibari *et al*. 2022). By combining the benefits of FGMs and electrostatic actuation, researchers can further advance the field of NEMS, enabling the development of novel devices with enhanced performance and functionality, (Al-Furjan *et al*. 2022, Zhao *et al*. 2023).

Regarding the mechanical behavior of smart functionally graded nanobeam structures, Tadi Beni, (2016) employed consistent size-dependent theory in the framework of the Euler-Bernoulli beam theory to analyze the bending, buckling, and free vibration behaviors of functionally graded (FG) piezoelectric nanobeams. Based on Eringen's nonlocal elasticity theory, Yan and Jiang (2017) provided a comprehensive review of the size-dependent mechanical analysis of piezoelectric nanostructures, incorporating surface elasticity, flexoelectricity influences. Chu *et al*. (2018) investigated the impact of flexoelectricity on the bending as well as vibration behaviors of FG piezoelectric nanobeams based on modified strain gradient theory (MNSGT). Nan *et al*. (2020) investigated the size-dependent static bending and free vibration behaviors of porous FG piezoelectric nanobeams. Ebrahimi *et al*. (2020) provided a comprehensive review of nanostructures exhibiting piezoelectric activity, focusing on their mechanical and electrical properties. Zhao *et al*. (2020) explored the combined effects of size-dependency, porosity, and axial gradation of FG materials on the behavior of flexoelectric modified couple stress Euler-Bernoulli nanobeams. Zhao *et al*. (2022) presented a comprehensive overview of size dependent dynamic behavior of piezoelectric micro/nanostructures. Ren *et al*. (2022) proposed strain/stress-driven integral nonlocal gradient piezoelectric models to analyze the bending behavior of FG piezoelectric nanobeams. In the framework of the generalized differential quadrature methodology, Zhao *et al*. (2022) analyzed the bending, free vibration, and buckling of axially functionally graded flexoelectric strain gradient nanobeams. Wang *et al*. (2023) investigated the electric response of piezoelectric curved beams, considering both direct piezoelectric and flexoelectric effects. Alshenawy *et al*. (2023) studied the nonlinear dynamics of micro-scale strain gradient piezoelectric bridge-type energy harvesters using a meshless collocation approach. Zou *et al*. (2023) explored the effects of thickness stretching and multi-field loading on the bending response of sandwich piezoelectric/piezomagnetic MEMS. Van Minh *et al*. (2023) reviewed the static and dynamic analysis of the flexoelectric effect in nanostructures, highlighting the major challenges and suggesting future research directions.

Zeng *et al*. (2020) developed a nonlocal strain gradient model to explore the dynamic behavior of piezoelectric sandwich nanobeam. Thongchom *et al*. (2022) investigated acoustic and fluid loading effects on multilayer cylindrical nanoshell with a functionally graded (FG) material core and PZ layers. Abdelrahman *et al*. (2023b) investigated the size dependent bending behavior of piezoelectric composite beam with perforated core on elastic foundation. The nonclassical buckling behavior of piezoelectric layered nanobeam with perforated core is analyzed by Abdelrahman *et al*. (2024a)

A literature survey reveals a significant gap in the understanding of the size-dependent electromechanical bending behavior of piezoelectric composite nanobeams with functionally graded porous cores, particularly when considering the combined effects of flexoelectricity and elastic foundation interactions. This study aims to fill this gap by developing a nonclassical model based on the modified nonlocal strain gradient theory to accurately analyze the size-dependent bending performance of these complex nanostructures. The primary objective of this research is to investigate the electromechanical bending behavior of piezoelectric layered nanobeams incorporating porous functionally graded cores and the influence of flexoelectricity. The study will explore the effects of various factors, such as material properties, geometric parameters, and loading conditions, on the electromechanical response of these nanostructures. The remainder of this paper is organized as follows: Section 2 presents the detailed modeling and formulation of the problem, including the development of the governing equations. Section 3 derives the electromechanical equilibrium equation, which incorporates the effects of nonlocality, strain gradients, and flexoelectricity. Section 4 outlines the proposed analytical solution strategy, which involves solving the governing equations using appropriate numerical techniques. Section 5 validates the accuracy of the developed solution procedure by comparing the results with existing analytical and numerical solutions. Section 6 presents the numerical results and a detailed discussion of the effects of various parameters on the electromechanical bending behavior of the nanobeam. Finally, Section 7 summarizes the key findings of the study and provides concluding remarks.

2. Modelling and formulation

A piezoelectric functionally graded porous (PFGP) nanocomposite beam structure with a span, L, width W_b, and height h_t is embedded in an elastic media and subjected to a partially distributed load of intensity, $Q(t)$, as shown in Fig. 1.

2.1 Functionally graded porous materials (FGPMs)

To model the nonhomogeneity distribution of the functionally graded material (FGM) properties of graded structures, there are different proposed distribution patterns in the literature, Eltaher *et al*. (2014), Wattanasakulpong and Chaikittiratana (2015), throughout this work study the Voigt model is employed, Attia and Abdelrahman (2018). According to this model the material property, $\Gamma(z)$ and volume fractions, $V_c\ (z)$, $V_m\ (z)$ of ceramic (c) and metal (m) constituents of FGM at any coordinate z is defined according to the rule of mixture as, Almitani *et al*. (2021), Abdelrahman *et al*. (2021)

$$\begin{Bmatrix} \Gamma(z) \\ V_c(z) \\ V_m(z) \end{Bmatrix} = \begin{Bmatrix} (\Gamma_c - \Gamma_m)V_c + \Gamma_m \\ \left(\frac{z}{h_c} + \frac{1}{2}\right)^n \\ 1 - V_c(z) \end{Bmatrix}, \tag{1}$$

To explore the impact of the material porosity distribution, three different types of porosity

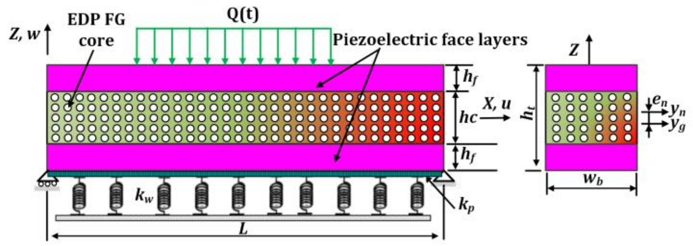

(a) Composite piezoelectric sandwich beam with Evenly distributed porosity (EDP) of porous FG core

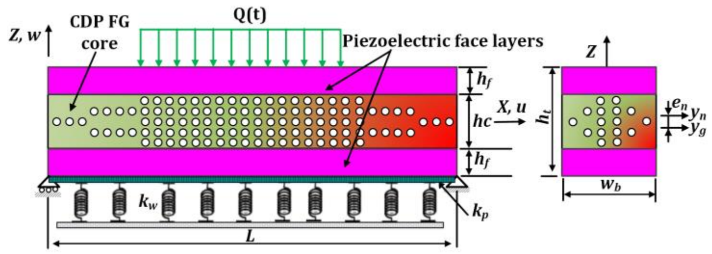

(b) Composite piezoelectric sandwich beam with Centrally distributed porosity (CDP) of porous FG core

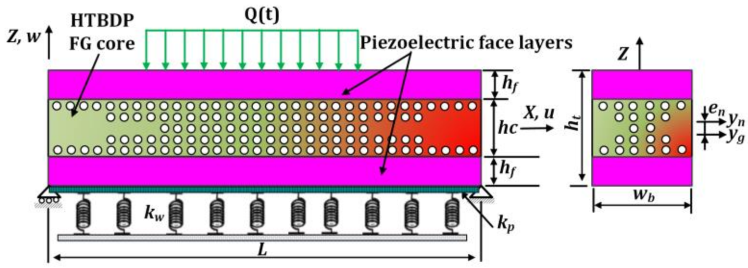

(c) Composite piezoelectric sandwich beam with High porosity distribution near the top and bottom surface (HTBDP) of porous FG core

Fig. 1 Piezoelectric functionally graded porous (PFGP) nanocomposite beam, with different porosity distribution patterns, embedded in an elastic media and subjected to partially distributed load, $Q(t)$

distribution patterns are considered, as shown in Fig. 1. According to Eq. (1) and the considered porosity distribution profiles, the physical as well as the mechanical properties of the functionally graded porous (FGP) nanobeam including Young's modulus, $E(z)$, Poisson's ratio, $v(z)$, shear modulus, $G(z)$, and mass density, $\rho(z)$, can be defined according to the porosity distribution profile type (1) (Evenly distributed porosity (EDP)) as, Mirjavadi *et al.* (2018), Alasadi *et al.* (2019), Dang and Do (2021), Nabawy *et al.* (2022), Assie *et al.* (2023), Esen *et al.* (2023), HS (2022), Yadav *et al.* (2023)

$$\begin{Bmatrix} E(z) \\ v(z) \\ G(z) \\ \rho(z) \end{Bmatrix} = \begin{Bmatrix} E_m + (E_c - E_m)\left(\frac{z}{h_c} + \frac{1}{2}\right)^n - \frac{\alpha}{2}(E_c + E_m) \\ v_m + (v_c - v_m)\left(\frac{z}{h_c} + \frac{1}{2}\right)^n - \frac{\alpha}{2}(v_c + v_m) \\ G_m + (G_c - G_m)\left(\frac{z}{h_c} + \frac{1}{2}\right)^n - \frac{\alpha}{2}(G_c + G_m) \\ \rho_m + (\rho_c - \rho_m)\left(\frac{z}{h_c} + \frac{1}{2}\right)^n - \frac{\alpha}{2}(\rho_c + \rho_m) \end{Bmatrix} \tag{2a}$$

On the other hand, according to the porosity distribution profile of type 2 (Centrally distributed porosity (CDP)), spatial variations of the FG core material properties throughout the thickness direction can be expressed as

$$\begin{Bmatrix} E(z) \\ v(z) \\ G(z) \\ \rho(z) \end{Bmatrix} = \begin{Bmatrix} E_m + (E_c - E_m)\left(\frac{z}{h_c} + \frac{1}{2}\right)^n - \frac{\alpha}{2}(E_c + E_m)\left(1 - \frac{2|z|}{h_c}\right) \\ v_m + (v_c - v_m)\left(\frac{z}{h_c} + \frac{1}{2}\right)^n - \frac{\alpha}{2}(v_c + v_m)\left(1 - \frac{2|z|}{h_c}\right) \\ G_m + (G_c - G_m)\left(\frac{z}{h_c} + \frac{1}{2}\right)^n - \frac{\alpha}{2}(G_c + G_m)\left(1 - \frac{2|z|}{h_c}\right) \\ \rho_m + (\rho_c - \rho_m)\left(\frac{z}{h_c} + \frac{1}{2}\right)^n - \frac{\alpha}{2}(\rho_c + \rho_m)\left(1 - \frac{2|z|}{h_c}\right) \end{Bmatrix} \tag{2b}$$

Furthermore, according to the porosity distribution profile of type 3 (High porosity distribution near the top and bottom surface (HTBDP)), variations of the FG core material characteristics through the transverse direction can be given by the following relations

$$\begin{Bmatrix} E(z) \\ v(z) \\ G(z) \\ \rho(z) \end{Bmatrix} = \begin{Bmatrix} E_m + (E_c - E_m)\left(\frac{z}{h_c} + \frac{1}{2}\right)^n - \frac{\alpha}{2}(E_c + E_m)\left(\frac{2|z|}{h_c}\right) \\ v_m + (v_c - v_m)\left(\frac{z}{h_c} + \frac{1}{2}\right)^n - \frac{\alpha}{2}(v_c + v_m)\left(\frac{2|z|}{h_c}\right) \\ G_m + (G_c - G_m)\left(\frac{z}{h_c} + \frac{1}{2}\right)^n - \frac{\alpha}{2}(G_c + G_m)\left(\frac{2|z|}{h_c}\right) \\ \rho_m + (\rho_c - \rho_m)\left(\frac{z}{h_c} + \frac{1}{2}\right)^n - \frac{\alpha}{2}(\rho_c + \rho_m)\left(\frac{2|z|}{h_c}\right) \end{Bmatrix} \tag{2c}$$

In which the subscripts c and m refer to ceramic and metal constituents of FG core, respectively. While n and α are the material gradation and porosity parameters, respectively.

2.2 The modified nonlocal strain gradient theory (MNSGT)

According to the modified nonlocal strain gradient theory MNSGT, the nonclassical constitutive equations for the components of the stress tensor, the higher order nonlocal stress tensor, and the nonlocal electric potential are expressed as, Mehralian *et al*. (2017), Basha *et al*. (2022), Esen *et al*. (2022)

$$(1 - (e_0 a)^2 \nabla^2)\sigma_{ij}^t = C_{ijkl}\left(1 - l^2 \frac{\partial^2}{\partial x^2}\right)\varepsilon_{kl} - e_{kij}E_k \tag{3a}$$

$$(1 - (e_0 a)^2 \nabla^2)\sigma_{ijl} = -\mu_{kijl}E_k \tag{3b}$$

$$(1 - (e_0 a)^2 \nabla^2)D_i = a_{ij}E_j + e_{ijk}\varepsilon_{jk} + \mu_{ijkl}\varepsilon_{jk,l} \tag{3c}$$

2.3 Piezoelectric nanobeams with flexoelectricity effect

Based on the EBBT, the displacement field and the associated kinematic relations can be expressed as, Zhao *et al.* (2020), Alazwari *et al.* (2022), Mohamed *et al.* (2024)

$$u_x(x,z,t) = u(x,t) - z\frac{\partial w(x,t)}{\partial x} \tag{4a}$$

$$u_z(x,z,t) = w(x,t) \tag{4b}$$

$$\varepsilon_{xx}(x,z,t) = \frac{\partial u_x(x,z,t)}{\partial x} = \frac{\partial u(x,t)}{\partial x} - z\frac{\partial^2 w(x,t)}{\partial x^2} \tag{4c}$$

where u_x (x, z, t), u_z (x, z, t) are the displacement field components in the spatial coordinate directions x and z, respectively. While $u(x,t)$ and $w(x,t)$ are the axial mid plane displacement and the transverse bending deflection. $\varepsilon_{xx}(x,z,t)$ represents the normal strain component. Including Poisson's effect, the constitutive relation of functionally graded materials can be written as, Abdelrahman *et al*. (2023a)

$$\begin{Bmatrix} \sigma_{xx}(x,z,t) \\ \sigma_{yy}(x,z,t) \\ \sigma_{zz}(x,z,t) \end{Bmatrix} = \begin{Bmatrix} \hat{E}(z)\varepsilon_{xx}(x,z,t) \\ \lambda(z)\varepsilon_{xx}(x,z,t) \\ \lambda(z)\varepsilon_{xx}(x,z,t) \end{Bmatrix} = \begin{Bmatrix} \big(2\mu(z)+\lambda(z)\big)\left(-z\frac{\partial^2 w(x,t)}{\partial x^2}\right) \\ \lambda(z)\left(-z\frac{\partial^2 w(x,t)}{\partial x^2}\right) \\ \left(\frac{\nu}{1-\nu}\right)\sigma_{xx}(x,z,t) \end{Bmatrix} \tag{5a}$$

where $\hat{E}(z)$ is the equivalent modulus of elasticity, $E(z)$ is the material elasticity modulus, ν is the Poisson's ratio, σ_{xx} (x, z, t), σ_{yy} (x, z, t), and σ_{zz} (x, z, t) are respectively the components of the Cauchy normal stress tensor, $\lambda(z)$ and $\mu(z)$ are Lame's constants in classical elasticity theory which are evaluated in terms of the material elasticity modulus, $E(z)$ and the Poisson's ratio, ν as follows

$$[\mu(z) \quad \lambda(z)] = \left[\frac{E(z)}{2(1+\nu)} \quad \frac{\nu E(z)}{(1+\nu)(1-2\nu)}\right] \tag{5b}$$

Regarding the electrical relations, the electric enthalpy energy density function is given by, Ansari *et al.* (2021), Ali *et al.* (2022)

$$H = -\frac{1}{2}a_{kl}E_k E_l + \frac{1}{2}c_{ijkl}\varepsilon_{ij}\varepsilon_{kl} - e_{ijk}\, E_k\, \varepsilon_{ij} - u_{ijkl}\, E_i\, \varepsilon_{jk,l} \tag{6}$$

Additionally, the electric displacement is expressed in terms of the electric enthalpy energy density, as Eftekhari *et al*. (2022), Liang *et al.* (2014)

$$D_i = -\frac{\partial H}{\partial E_i} = a_{ij}E_j + e_{ijk}\, \varepsilon_{jk} + u_{ijkl}\, \varepsilon_{jk,l} \tag{7}$$

with E_i refers to the electric fields is given by Ali *et al*. (2022)

$$E_i = -\frac{\partial \phi_i}{\partial x_i} \tag{8}$$

where $a_{kl}, c_{ijkl}, e_{ijk},$ and u_{ijkl} respectively refer to the 2nd order permittivity tensor, the fourth order elasticity tensor, the piezoelectric coefficient tensor, and the electric field strain gradient coupling coefficient which denotes the higher order electromechanical coupling induced by strain gradients. The Cartesian component of the electric displacement can be evaluated as, Zeng *et al*. (2020), Abdelrahman *et al*. (2024a)

$$D_z(x,z,t) = a_{33}E_z(x,z,t) + e_{311}\, \varepsilon_{xx}(x,z,t) + u_{3111}\varepsilon_{xx,x}(x,z,t) + u_{3113}\varepsilon_{xx,z}(x,z,t) \tag{9}$$

Based on the Gaussian theorem, the following condition is verified:-

$$D_{z,z}(x,z,t) = 0 \Rightarrow a_{33}E_{z,z}(x,z,t) + e_{311}\varepsilon_{xx,z}(x,z,t) + u_{3111}\varepsilon_{xx,xz}(x,z,t) + u_{3113}\varepsilon_{xx,zz}(x,z,t) = 0 \tag{10}$$

Rearranging terms in Eq. (10) one can write

$$E_{z,z}(x,z,t) = \frac{-1}{a_{33}}\left\{e_{311}\varepsilon_{xx,z}(x,z,t) + u_{3111}\varepsilon_{xx,xz}(x,z,t) + u_{3113}\varepsilon_{xx,zz}(x,z,t)\right\} \tag{11}$$

Integrating Eq. (11) w.r.t z yields

$$E_z(x,z,t) - E_{z0} = \frac{-1}{a_{33}}\left\{e_{311}\varepsilon_{xx}(x,z,t) + u_{3111}\varepsilon_{xx,x}(x,z,t) + u_{3113}\varepsilon_{xx,z}(x,z,t)\right\} \tag{12}$$

Considering only the bending effect, Eq. (12) can be expressed in terms of $w(x,t)$ as

$$E_z(x,z,t) = E_{z0} + \frac{z}{a_{33}}\left[e_{311}\left(\frac{\partial^2 w(x,t)}{\partial x^2}\right) + u_{3111}\left(\frac{\partial^3 w(x,t)}{\partial x^3}\right)\right] \tag{13}$$

with E_{z0} refers to the initial electric field in the *z*-direction.

3. Estableshment of the electromechanical equilibrium equation

Applying Hamilton's principle, the electromechanical equilibrium equation can be expressed as, Abdelrahman *et al*. (2014), Abdelrahman *et al*. (2024b)

$$-\int_{t_1}^{t_2}[\delta\Pi + \delta W_{ex}]\,dt = 0 \tag{14}$$

where Ω refers to the volume of the composite beam, Π is the electroelastic strain energy which could be expressed for Euler Bernoulli beam theory (EBBT) as, Eltaher *et al.* (2021)

$$\Pi = \frac{1}{2}\int_\Omega\Big(\sigma_{xx}^t(x,z,t)\varepsilon_{xx}(x,z,t) - D_z(x,z,t)E_z(x,z,t) + \sigma_{111}\varepsilon_{xx,x}(x,z,t) + \sigma_{113}\varepsilon_{xx,z}(x,z,t)\Big)d\Omega = \frac{1}{2}\int_0^L\left(\bar{M}\varepsilon_{xx0} + \bar{M}'\varepsilon_{xx0,x}\right)dx \tag{15}$$

in which

$$\begin{bmatrix}\varepsilon_{xx0} & \bar{M} & \bar{M}'\end{bmatrix} = \begin{bmatrix}-\frac{\partial^2 w}{\partial x^2} & M + \frac{e_{311}}{a_{33}}M_D + N_{113} & \frac{\mu_{3111}}{a_{33}}M_D + N_{111}\end{bmatrix} \tag{16}$$

Utilizing Eq. (16), the electroelastic strain energy can be expressed as

$$\Pi = \frac{1}{2}\int_0^L\left[\left(M + \frac{e_{311}}{a_{33}}M_D + N_{113}\right)\left(-\frac{\partial^2 w}{\partial x^2}\right) + \left(\frac{\mu_{3111}}{a_{33}}M_D + N_{111}\right)\left(-\frac{\partial^3 w}{\partial x^3}\right)\right]\mathrm{d}x \tag{17}$$

Recalling the modified nonlocal strain gradient theory, the resultant forces and moments can be given by the following relations, Hosseini *et al.* (2020)

$$\left(1 - (e_0 a)^2\frac{\partial^2}{\partial x^2}\right)\begin{Bmatrix}M\\ N_{113}\\ M_{111}\\ M_D\end{Bmatrix} = \begin{Bmatrix}\left(1 - l^2\frac{\partial^2}{\partial x^2}\right)\left\{\mathcal{D} - E_p I_p\right\}\varepsilon_{xx0} + \frac{e_{311}^2}{a_{33}}I_p\varepsilon_{xx} + \frac{e_{311}\mu_{3111}I_p}{a_{33}}\frac{\partial\varepsilon_{xx0}}{\partial x} - e_{311}I_1E_{z0}\\ 0\\ w_b\left\{\frac{\mu_{3111}}{a_{33}}I_p\left(e_{311}\varepsilon_{xx0} + \mu_{3111}\frac{\partial\varepsilon_{xx0}}{\partial x}\right) - \mu_{3111}I_1E_{z0}\right\}\\ w_b a_{33}I_1E_{z0}\end{Bmatrix} \tag{18}$$

in which

$$\begin{aligned}&[\mathcal{D} \quad I_p \quad I_1 \quad A_c \quad A_p] = \\ &\left[\int_{-h_c/2}^{h_c/2}(z-e_n)^2 w_b E(z)dz \quad \left(\frac{h^3}{12}-I_c\right) \quad \left(\frac{h^2}{4}-\frac{h_c^2}{4}\right) \quad h_c w_b \quad h_p w_b\right]\end{aligned} \tag{19}$$

with w_b is the beam width, e_n locates the shift distance of the neutral plane from the geometric mid plane. This shift could be obtained for evenly distributed porosity (EDP) from the following relation

$$e_{n_{EDP}} = \frac{\int_A zE(z)_{EDP}dA}{\int_A E(z)_{EDP}dA} = \frac{\int_{-h_c/2}^{h_c/2} zE(z)_{EDP}dz}{\int_{-h_c/2}^{h_c/2} E(z)_{EDP}dz} = \frac{h_c n(E_c-E_m)}{2(n+2)\left(nE_m+E_c-\frac{\alpha}{2}(n+1)(E_c+E_m)\right)} \tag{20}$$

for centrally distributed porosity (CDP) the neutral plane is located by the following relation

$$e_{n_{CDP}} = \frac{\int_A zE(z)_{CDP}dA}{\int_A E(z)_{CDP}dA} = \frac{\int_{-h_c/2}^{h_c/2} zE(z)_{CDP}dz}{\int_{-h_c/2}^{h_c/2} E(z)_{CDP}dz} = \frac{h_c n(E_c-E_m)}{2(n+2)\left\{nE_m+E_c-\frac{\alpha}{4}(n+1)(E_c+E_m)\right\}} \tag{21}$$

On the other hand considering the high porosity distribution near the top and bottom surface (HTBDP), the neutral plane is expressed as follows

$$e_{n_{HTBDP}} = \frac{\int_A zE(z)_{HTBDP}dA}{\int_A E(z)_{HTBDP}dA} = \frac{\int_{-h_c/2}^{h_c/2} zE(z)_{HTBDP}dz}{\int_{-h_c/2}^{h_c/2} E(z)_{HTBDP}dz} = \frac{h_c n(E_c-E_m)}{2(n+2)\left[nE_m+E_c-\frac{\alpha}{4}(n+1)(E_c+E_m)\right]} \tag{22}$$

On the other hand, the equivalent bending stiffness of the porous FG core for evenly distributed porosity (EDP), $\mathcal{D}_{EDP}$ can be expressed as follows

$$\begin{aligned}\mathcal{D}_{EDP} &= \int_{-h_c/2}^{h_c/2}\left(z-e_{n_{EDP}}\right)^2 w_b E_{EDP}(z)dz = w_b\left[\frac{E_m}{3}\left(\left(\frac{h_c}{2}-e_{n_{EDP}}\right)^3+\left(\frac{h_c}{2}+e_{n_{EDP}}\right)^3\right)+\right. \\ &\left\{\frac{h_c(E_c-E_m)}{(n+1)}\right\}\left\{\left(\frac{h_c}{2}-e_{n_{EDP}}\right)^2-\left\{\frac{2h_c}{(n+2)}\right\}\left(\frac{h_c}{2}-e_{n_{EDP}}\right)+\left\{\frac{2(h_c)^2}{(n+2)(n+3)}\right\}\right\}-\frac{\alpha}{6}(E_c+E_m)\left\{\left(\frac{h_c}{2}-\right.\right. \\ &\left.\left.\left.e_{n_{EDP}}\right)^3+\left(\frac{h_c}{2}+e_{n_{EDP}}\right)^3\right\}\right]\end{aligned} \tag{23}$$

Further, for centrally distributed porosity (CDP), the equivalent bending stiffness, $\mathcal{D}_{CDP}$ can be expressed as follows

$$\begin{aligned}\mathcal{D}_{CDP} &= \int_{-h_c/2}^{h_c/2}\left(z-e_{n_{CDP}}\right)^2 w_b E_{CDP}(z)dz = w_b\left[\frac{E_m}{3}\left(\left(\frac{h_c}{2}-e_{n_{CDP}}\right)^3+\left(\frac{h_c}{2}+e_{n_{CDP}}\right)^3\right)+\right. \\ &\left\{\frac{h_c(E_c-E_m)}{(n+1)}\right\}\left\{\left(\frac{h_c}{2}-e_{n_{CDP}}\right)^2-\left\{\frac{2h_c}{(n+2)}\right\}\left(\frac{h_c}{2}-e_{n_{CDP}}\right)+\left\{\frac{2(h_c)^2}{(n+2)(n+3)}\right\}\right\}-\frac{\alpha}{12}\frac{(E_c+E_m)}{h_c}\left\{\left(\frac{h_c}{2}+\right.\right. \\ &\left.\left.\left.e_{n_{CDP}}\right)^4+\left(\frac{h_c}{2}-e_{n_{CDP}}\right)^4-2\left(e_{n_{CDP}}\right)^4\right\}\right]\end{aligned} \tag{24}$$

Furthermore, considering the high porosity distribution near the top and bottom surface (HTBDP), the equivalent bending stiffness, $\mathcal{D}_{HTBDP}$ can be derived as follows

$$\begin{aligned}\mathcal{D}_{HTBDP} &= \int_{-h_c/2}^{h_c/2}\left(z-e_{n_{HTBDP}}\right)^2 w_b E_{HTBDP}(z)dz = w_b\left[\frac{E_m}{3}\left(\left(\frac{h_c}{2}-e_{n_{HTBDP}}\right)^3+\left(\frac{h_c}{2}+\right.\right.\right. \\ &\left.\left.e_{n_{HTBDP}}\right)^3\right)+\left\{\frac{h_c(E_c-E_m)}{(n+1)}\right\}\left\{\left(\frac{h_c}{2}-e_{n_{HTBDP}}\right)^2-\left\{\frac{2h_c}{(n+2)}\right\}\left(\frac{h_c}{2}-e_{n_{HTBDP}}\right)+\right.\end{aligned}$$

$$\left.\frac{2(h_c)^2}{(n+2)(n+3)}\right\} - \frac{\alpha}{6}(E_c + E_m)\left\{\left(\frac{h_c}{2} + e_{n_{HTBDP}}\right)^3 + \left(\frac{h_c}{2} - e_{n_{HTBDP}}\right)^3\right\} + \frac{\alpha}{12}\left(\frac{E_c+E_m}{h_c}\right)\left\{\left(\frac{h_c}{2} + e_{n_{HTBDP}}\right)^4 + \left(\frac{h_c}{2} - e_{n_{HTBDP}}\right)^4 - 2\left(e_{n_{HTBDP}}\right)^4\right\}\Bigg] \tag{25}$$

The work done by the applied external transverse loads and the elastic foundation could be expressed as follows (Siam *et al.* 2023, Mohamed *et al.* 2024)

$$W_{ex} = -w_b \int_0^L \left\{q(x,t)D_s(x - x_p) + \left[k_w w(x,t) - k_p \frac{\partial^2 w(x,t)}{\partial x^2}\right]\right\} w(x,t)\, dx \tag{26}$$

with $D_s(.)$ refers to the Dirac delta function, and x is the abscissa, measured from the left end of the beam, $q(x,t)$ is the applied external shear force, k_w, k_p are respectively refer to the Winkler and the Pasternak foundation parameters.

Recalling Eqs. (17) & (26) into Eq. (14) and evaluate the integrals, the coupled equilibrium equation can be expressed as follows

$$-\int_{t_1}^{t_2}[\delta\Pi + \delta W_{ex}]\, dt = -\int_{t_1}^{t_2}\left[\int_0^L\left[\left(M + \frac{e_{311}}{a_{33}}M_D + N_{113}\right)\delta\left(-\frac{\partial^2 w}{\partial x^2}\right) + \left(\frac{\mu_{3111}}{a_{33}}M_D + N_{111}\right)\delta\left(-\frac{\partial^3 w}{\partial x^3}\right)\right] \mathrm{dx} + w_b\int_0^L\left\{q(x,t)D_s(x - x_p) + \left[k_w w(x,t) - k_p \frac{\partial^2 w(x,t)}{\partial x^2}\right]\right\}\delta w(x,t)\, dx\right] dt = 0 \tag{27a}$$

Evaluating integrals yields

$$\frac{\partial^2 \bar{M}}{\partial x^2} - \frac{\partial^3 \bar{M}'}{\partial x^3} = \left\{q(x,t) + \left[k_w w(x,t) - k_p \frac{\partial^2 w(x,t)}{\partial x^2}\right]\right\} \tag{27b}$$

For convenience, the coupled equilibrium equation is expressed in terms of normalized variables. For this purpose the following nondimensional parameters are defined

$$[W \quad X \quad \bar{q}] = \left[\frac{w}{h_t} \quad \frac{x}{L} \quad \frac{qL^3}{([E_c I_c]_{eq} + E_p I_p)}\right] \tag{28a}$$

$$\left[dx \quad \frac{dw}{dX} \quad \frac{d^4 w}{dx^4} \quad \frac{d^6 w}{dx^6}\right] = \left[L dX \quad \left(\frac{h_t}{L}\right)\frac{dW}{dX} \quad \left(\frac{h_t}{L^4}\right)\frac{d^4 W}{dX^4} \quad \left(\frac{h_t}{L^6}\right)\frac{d^6 W}{dX^6}\right] \tag{28b}$$

Substituting Eqs. (18) and (28) into Eq. (27b) the coupled equilibrium equation can be expressed in terms of the normalized bending deflection as follows

$$-\left[\left\{\mathcal{D} + E_p I_p\right\} + I_p \frac{e_{311}^2}{a_{33}}\right]\left(\frac{h}{L^4}\right)\left[\frac{d^4 W(X)}{dX^4}\right] + \left(l^2\left[\mathcal{D} - E_p I_p\right] + I_p \frac{\mu_{3111}^2}{a_{33}}\right)\left(\frac{h}{L^6}\right)\frac{\partial^6 W(X)}{\partial X^6} = \left(1 - \frac{(e_0 a)^2}{L^2}\frac{\partial^2}{\partial X^2}\right)\left[q(X) + \left[hk_w W(X) - \frac{hk_p}{L^2}\frac{d^2 W(X)}{dX^2}\right]\right] \tag{29}$$

4. Solution technique

The coupled electromechanical system defined by the equilibrium Eq. (29) is to be solved to investigate the size dependent electromechanical bending behavior of composite nanobeam with porous functionally graded core layered with two symmetrical piezoelectric face layers embedded in an elastic medium. Considering the simply supported beam, the following boundary conditions are to be satisfied

$$\begin{Bmatrix} W(X) \\ \frac{d^2W(X)}{dX^2} \end{Bmatrix}_{at\ X=0} = \begin{Bmatrix} W(X) \\ \frac{d^2W(X)}{dX^2} \end{Bmatrix}_{at\ X=1} = 0 \tag{30}$$

The transverse bending deflection, its derivatives w. r. to X as well as the applied external load can be expanded by Fourier expansion in the following forms, Alazwari *et al.* (2022), Abdelrahman and Eltaher (2022)

$$\begin{Bmatrix} W(X) & \frac{d^2W(X)}{dX^2} \\ \frac{d^4W(X)}{dX^4} & \frac{d^6W(X)}{dX^6} \\ q(X) & \frac{d^2q(X)}{dX^2} \end{Bmatrix} = \begin{Bmatrix} \sum_{n=1}^{\infty} W_n \sin(n\pi X) & -\sum_{n=1}^{\infty}(n\pi)^2 W_n \sin(n\pi X) \\ \sum_{n=1}^{\infty}(n\pi)^4 W_n \sin(n\pi X) & -\sum_{n=1}^{\infty}(n\pi)^6 W_n \sin(n\pi X) \\ \sum_{n=1}^{\infty} Q_n \sin(n\pi X) & -\sum_{n=1}^{\infty}(n\pi)^2 Q_n \sin(n\pi X) \end{Bmatrix} \tag{31}$$

where Q_n is the Fourier expansion coefficients which depends on the applied loading profile. For uniformly distributed load

$$Q_n = \begin{cases} \frac{2q_0}{(n\pi)}(1-\cos n\pi) & \text{Uniformly distributed load with intensity } q_0 \\ \frac{2P}{L} sin(n\pi\bar{x}_p) & \text{Point load of intensity } PD(X-\bar{x}_p) \text{ applied at a distance } \bar{x}_p \end{cases} \tag{32}$$

Substituting Eqs. (34), (35), (36) and (37) into Eq. (33) yields

$$\left[\sum_{n=1}^{\infty}\left\{\left[\{\mathcal{D}+E_pI_p\}+I_p\frac{e_{311}^2}{a_{33}}\right]\left(\frac{h}{L^4}\right)(n\pi)^4+\left(l^2[\mathcal{D}-E_pI_p]+I_p\frac{\mu_{3111}^2}{a_{33}}\right)\left(\frac{h}{L^6}\right)(n\pi)^6+\left\{\left(k_wh+\frac{hk_p}{L^2}(n\pi)^2\right)\left(1+\frac{(e_0a)^2}{L^2}(n\pi)^2\right)\right\}\right\}W_n\sin(n\pi X)\right]=-\sum_{n=1}^{\infty}\left(1+\frac{(e_0a)^2}{L^2}\right)Q_n\sin(n\pi X) \tag{33}$$

Simplifying Eq. (33) the nondimesional size dependent electromechanical bending deflection profile, $W^{NELECM}(X)$ is derived as

$$W^{NELECM}(X) = \sum_{n=1}^{\infty}\frac{-\left(1+\frac{(e_0a)^2}{L^2}(n\pi)^2\right)Q_n\sin(n\pi X)}{\left\{\left(\frac{h}{L^4}\right)(n\pi)^4\left(\left[\{\mathcal{D}+E_pI_p\}+I_p\frac{e_{311}^2}{a_{33}}\right]+\left(l^2[\mathcal{D}+E_pI_p]+I_p\frac{\mu_{3111}^2}{a_{33}}\right)\left(\frac{n\pi}{L}\right)^2\right)+\left(1+\frac{(e_0a)^2}{L^2}(n\pi)^2\right)\left(k_wh+\frac{hk_p}{L^2}(n\pi)^2\right)\right\}} \tag{34}$$

Neglecting the electrical effects, the nonclassical mechanical transverse bending deflection profile, $W^{NMEC}(X)$ could be expressed as

$$W^{NMEC}(X) = \sum_{n=1}^{\infty}\frac{-\left(1+\frac{(e_0a)^2}{L^2}(n\pi)^2\right)Q_n\sin(n\pi X)}{\left\{\left(\frac{h}{L^4}\right)(n\pi)^4\left([\{(D_2)_{eq}\}]+(l^2[(D_2)_{eq}])\left(\frac{n\pi}{L}\right)^2\right)+\left(1+\frac{(e_0a)^2}{L^2}(n\pi)^2\right)\left(k_wh+\frac{hk_p}{L^2}(n\pi)^2\right)\right\}} \tag{35}$$

5. Validation of the developed strategy

The accuracy of the developed model and the solution strategy is validated through this section.

Table 1 The nonlocal strain gradient maximum nondimensional deflection parameter, $w_q = 10^2 \times w_{qmax}\left(\frac{EI}{\mathrm{qL}^4}\right)$ of homogeneous elastic simply supported beam at different values of normalized size and local parameters, (l/h), (e_0a/h) and different beam slenderness ratio for uniformly distributed load of intensity q for E=70 GPa, ν=0.3, b=h=1 nm

L/h	Normalized nonlocal parameter (e_0a/h)	Normalized size parameter, (l/h)					
		0		1		2	
		Present	Lu *et al.* (2017)	Present	Lu *et al.* (2017)	Present	Lu *et al.* (2017)
10	0	1.302083	1.3021	1.186949	1.1870	0.935992	0.9360
	1	1.427083	1.4271	1.302083	1.3021	1.027515	1.0275
	2	1.802083	1.8021	1.647488	1.6475	1.302083	1.3021
20	0	1.302083	1.3021	1.271458	1.2715	1.186949	1.1870
	1	1.333333	1.3333	1.302083	1.3021	1.215732	1.2157
	2	1.427083	1.4271	1.393959	1.3940	1.302083	1.3021
50	0	1.302083	1.3021	1.297099	1.2971	1.282339	1.2823
	1	1.307083	1.3071	1.302083	1.3021	1.287275	1.2873
	2	1.322083	1.3221	1.317035	1.3170	1.302083	1.3021

Four different validation cases are presented. The 1st case compared the nonlocal strain gradient maximum nondimensional transverse bending parameters, w_q of SS homogeneous elastic nanobeam under uniformly distributed load of intensity q. Additionally, the 2nd validation case concerns with comparison of the nonlocal maximum nondimensional bending parameter, w_q of SS FG nanobeam under uniformly distributed load. Further, the 3rd case aims to compare the maximum classical nondimensional bending parameter, w_P of SS porous FG beam under point load. Furthermore, the 4th case compared the maximum nondimensional bending deflection, w_q of SS homogeneous beam rested on an elastic foundation under uniformly distributed load.

Comparison of the nonlocal strain gradient maximum nondimensional bending parameter, $w_q = 10^2 \times w_{qmax}\left(\frac{EI}{\mathrm{qL}^4}\right)$ of SS homogeneous nanobeams at different values of normalized microstructure size and nonlocal parameters, (l/h) and (e_0a/h) for different beam slenderness ratio, (L/h) is depicted in Table 1. It is demonstrated that, for the three considered sets of beam slenderness ratios, an excellent agreement is revealed between the results of the present strategy and the corresponding cases obtained by Lu *et al.* (2017) which outlines the high accuracy and reliability of the present model in predicting size dependent flexural behavior of isotropic nanobeams.

Results of the present procedure for the nonlocal maximum nondimensional deflection parameter, w_q for SS FG nanobeam at different values of normalized nonlocal parameter, ea/h, material gradation index, n and beam slenderness ratio, (L/h) for uniformly distributed load are compared with the corresponding results reported by Simsek and Yurtcu, (2013) in Table 2. It is seen that there is an excellent agreement for the considered cases with the corresponding cases detected by Simsek and Yurtcu, (2013) which demonstrates the accuracy of the developed procedure.

The accuracy of the developed procedure to accurately investigate the bending behavior of porous FG beam is demonstrated in Table 3. Comparison of the maximum nondimensional

Table 2 The nonlocal maximum nondimensional deflection parameter, $w_q = 10^2 \times w_{max}\left(\frac{E_m I}{qL^4}\right)$ of simply supported FG nanobeam at different values of material gradation index, n, normalized nonlocal parameter, (e_0a/h), and different beam slenderness ratio, (L/h) for uniformly distributed load for E_1=1 TPa, E_2=0.25 TPa, v_1=v_2=0.3, b=h=1 nm

L/h	Grad. Index, n	Normalized nonlocality parameter, (e_0a/h)									
		0		0.5		1.0		1.5		2	
		Present	Simsek and Yurtcu (2013)	Present	Simsek and Yurtcu (2013)	Present	Simsek and Yurtcu (2013)	Present	Simsek and Yurtcu (2013)	Present	Simsek and Yurtcu (2013)
10	0	5.208333	5.2083	5.333333	5.3333	5.708333	5.7083	6.333333	6.3333	7.208332	7.2083
	0.3	3.1387	3.14.1	3.214029	3.2154	3.440016	3.4415	3.816659	3.8183	4.343961	4.3459
	1	2.367424	2.3674	2.424242	2.4242	2.594697	2.5946	2.878788	2.8787	3.276515	3.2765
	3	1.884976	1.8849	1.930215	1.9302	2.065933	2.0659	2.29213	2.2921	2.608806	2.6088
	10	1.545035	1.5450	1.582116	1.5821	1.693358	1.6933	1.878762	1.8787	2.138328	2.1383
30	0	5.208333	5.2083	5.222222	5.2222	5.263889	5.2638	5.333333	5.3333	5.430555	5.4305
	0.3	3.1387	3.14.1	3.14707	3.1484	3.17218	3.1736	3.214029	3.2154	3.272618	3.2740
	1	2.367424	2.3674	2.373737	2.3737	2.392677	2.3926	2.424242	2.4242	2.468434	2.4684
	3	1.884976	1.8849	1.890002	1.8900	1.905082	1.9095	1.930215	1.9302	1.965401	1.9654
	10	1.545035	1.5450	1.549155	1.5491	1.561515	1.5615	1.582116	1.5821	1.610956	1.6109
100	0	5.208333	5.2083	5.209583	5.2095	5.213333	5.2133	5.219583	5.2195	5.228333	5.2283
	0.3	3.1387	3.14.1	3.139454	3.1408	3.141714	3.1431	3.14548	3.1468	3.150753	3.1521
	1	2.367424	2.3674	2.367992	2.3679	2.369697	2.3696	2.372538	2.3725	2.376515	2.3765
	3	1.884976	1.8849	1.885428	1.8854	1.886785	1.8876	1.889047	1.8890	1.892214	1.8922
	10	1.545035	1.5450	1.545406	1.5454	1.546518	1.5465	1.548372	1.5483	1.550968	1.5509

Table 3 The maximum nondimensional deflection parameter, $w_P = 10^3 \times \mathrm{w}_{max}\left(\frac{\mathrm{E}_m \mathrm{I}}{\mathrm{PL}^3}\right)$ of porous FG simply supported beam for (EPD) at different values of material gradation index, n and porosity parameter, (α) and different beam aspect ratio for point load for E_m=70 GPa, E_c=380 GPa, v_m=v_c=0.3, b=h

L/h	*Grad. Index, n*	Porosity parameter, α					
		0		0.1		0.2	
		Present	Rahmani *et al.* (2020) FE	Present	Rahmani *et al.* (2020) FE	Present	Rahmani *et al.* (2020) FE
5	0.2	4.680874	4.659	5.051442	5.027	5.48615	5.458
	1	7.699451	7.692	8.933856	8.938	10.657851	10.743
	2	9.867064	9.873	12.24319	12.323	16.197004	16.864
	5	11.667709	11.702	15.172483	----	21.795661	-----
20	0.2	4.680874	4.660	5.051442	5.027	5.48615	5.458
	1	7.699451	7.692	8.933856	8.938	10.657851	10.743
	2	9.867064	9.873	12.24319	12.323	16.197004	16.864
	5	11.667709	11.702	15.172483	-----	21.795661	-----

Table 4 Comparison of the maximum nondimensional central bending deflection w for simply supported (SS) beam rested on an elastic foundation under uniformly distributed load of intensity q for beam aspect ratios, L/h =120, 15, 5 at different values of the elastic foundation parameters for ν=0.3, E=70 GPa, b=h

Slenderness ratio, (L/h)	Foundation Parameters		Method of Solution				
	K_w	K_p	Present	Chen *et al.* (2004)	Ying *et al.* (2008)	Fahsi *et al.* (2019)	Atmane *et al.* (2017)
120	0	0	1.302083	1.302290	1.30229	1.30218	1.30090
		10	0.644771	0.644827	0.64483	0.64483	0.64461
		25	0.366091	0.366111	0.36611	0.36612	0.36621
	10	0	1.180396	1.180567	1.18057	1.18048	1.17944
		10	0.613275	0.613325	0.61333	0.61333	0.61315
		25	0.355649	0.355668	0.35567	0.35568	0.35578
	10^2	0	0.64002	0.640074	0.64007	0.64005	0.63987
		10	0.425557	0.425582	0.42558	0.42559	0.42563
		25	0.282834	0.282846	0.28285	0.28360	0.28302
15	0	0	1.302083	1.31528	1.31527	1.30840	1.30226
		10	0.644771	0.64835	0.64830	0.64853	0.65329
		25	0.366091	0.36742	0.36735	0.36742	0.37968
	10	0	1.180396	1.19140	1.19134	1.19140	1.18173
		10	0.613275	0.61656	0.61649	0.61673	0.62233
		25	0.355649	0.35692	0.35684	0.35780	0.36944
	10^2	0	0.64002	0.64377	0.64343	0.64217	0.64864
		10	0.425557	0.42741	0.42716	0.42744	0.43801
		25	0.282834	0.28380	0.28360	0.28428	0.29812
5	0	0	1.302083	1.420261	1.42024	1.35992	1.31338
		10	0.644771	0.678202	0.67451	0.68980	0.72171
		25	0.366091	0.381703	0.37667	0.38980	0.48428
	10	0	1.180396	1.282598	1.27731	1.22991	1.20032
		10	0.613275	0.646391	0.64025	0.64678	0.69452
		25	0.355649	0.372064	0.36568	0.37818	0.47554
	10^2	0	0.64002	0.696100	0.66848	0.65950	0.71779
		10	0.425557	0.459267	0.43881	0.44373	0.53449
		25	0.282834	0.305161	0.28944	0.29791	0.41489

bending parameter for SS porous FG beam, with uniform porosity distribution model, under concentrated central point load for different porosity and material gradation parameters at L/h= 5, 20 is shown in Table 3. It is observed that good agreement is found between the present model results and the corresponding cases reported by Rahmani *et al.* (2020).

Regarding the validation of bending behavior of beams embedded in an elastic media, Table 4 presents a comparison of the obtained maximum normalized bending deflection parameter with the corresponding results reported in the literature. The following nondimensional parameters are

Table 5 The piezoelectrically layered functionally graded nanobeam geometrical and material parameters (Zeng *et al*. 2020, Hosseini-Hashemi *et al*. 2014)

Parameters		Thickness (nm)	Length (nm)	Width (nm)	Young's Modulus (GPa)	Mass Density (Kg/m³)	Poisson's ratio	e_{311} (C/m²)	μ_{3111} (C/m)	a_{33} N/(m².K)
FGM Core	Metal	1.6	40	2	70	2700	0.3	----	----	------
	Ceramic				210	2370	0.3	----	----	------
Piezoelectric Layer		0.2	40	2	132	7500	0.27	-4	5×10^{-8}	7.124×10^{-9}

utilized: the central deflection parameter is defined: $w = w_{max}\left(\frac{E_{eq}I}{qL^4}\right)$ where E_{eq} is the equivalent elasticity modulus which can be expressed as, $E_{eq} = \frac{\nu E}{(1+\nu)(1-2\nu)} + \frac{E}{(1+\nu)}$. The nondimensional elastic foundation parameters are defined as, $K_w = \frac{k_w L^4}{E_{eq}I}$ and $K_p = \frac{k_p L^2}{E_{eq}I}$. with q is the intensity of the distributed load, I is the 2nd moment of area of the beam cross section, L is the beam length. By comparing the maximum nondimensional central deflection of simply supported beams subjected to a uniformly distributed load for various foundation parameter values, it is noticed that there is an excellent agreement with the results reported in the literature by (Chen *et al*. 2004, Ying *et al*. 2008, Fahsi *et al*. 2019, Atmane *et al*. 2017). This strong correlation validates the developed analytical strategy.

6. Results and discussions

To demonstrate the effectiveness of the verified proposed solution strategy to efficiently investigate the size dependent bending behavior of piezoelectrically layered sandwich nanobeam with porous functionally graded core embedded in an elastic medium, consider a simply supported (SS) beam with the geometrical and material characteristics presented in Table 5. Both uniformly distributed load with intensity, q=1 N/m and concentrated central point load of intensity P=q×L are considered and analyzed. Intensive numerical experiments are conducted to comprehensively investigate the impacts of the different mechanical as well as the electrical parameters on the nonclassical electromechanical as well as the mechanical bending responses of porous functionally graded composite nanobeams layered with piezoelectric layers embedded in an elastic medium.

The normalized parameters presented in Table 6 are utilized through presentation of numerical results.

Table 6 The normalized parameters

	$\mathrm{w}_q \times 10^2$	$\mathrm{w}_p \times 10^2$	K_w	K_p
Electromechanical (Elecmech)	$w_{maxq}\left(\frac{(E_eI)_{cceq}+(E_eI)_p}{qL^4}\right)$	$w_{maxp}\left(\frac{(E_eI)_{cceq}+(E_eI)_p}{pL^3}\right)$	$\frac{k_wL^4}{(E_eI)_{cmeq}+(E_eI)_p}$	$\frac{k_pL^2}{(E_eI)_{cmeq}+(E_eI)_p}$
Mechanical (Mech) (h_p=0, h=h_c)	$w_{maxq}\left(\frac{(E_eI)_{cmeq}}{qL^4}\right)$	$w_{maxp}\left(\frac{(E_eI)_{cmeq}}{pL^3}\right)$	$\frac{k_wL^4}{(E_eI)_{cmeq}}$	$\frac{k_pL^2}{(E_eI)_{cmeq}}$

with w_q and w_p are respectively the normalized bending parameter due to uniformly and concentrated loads. K_w and K_p are the normalized elastic foundation parameters, E_e is the equivalent elasticity modulus, $(E_eI)_{mceq}$ and $(E_eI)_{cceq}$ are respectively the equivalent rigidity of the metallic and ceramic materials.

6.1 Effect of the material porosity

Porosity of the functionally graded materials significantly affects the bending behavior of nanobeams. To capture this effect, different porosity distribution models with different porosity index are investigated. Dependency of the bending behavior on the material porosity parameter, α at different material gradation index for different material porosity distribution models for uniformly distributed and point loading conditions is depicted in Fig. 2. It is observed that, due to the decrement of the overall system stiffness, the bending deflection parameters increase with increasing the porosity parameter for both electromechanical and mechanical behaviors. Additionally, because of increasing the core material metal content, increasing the material

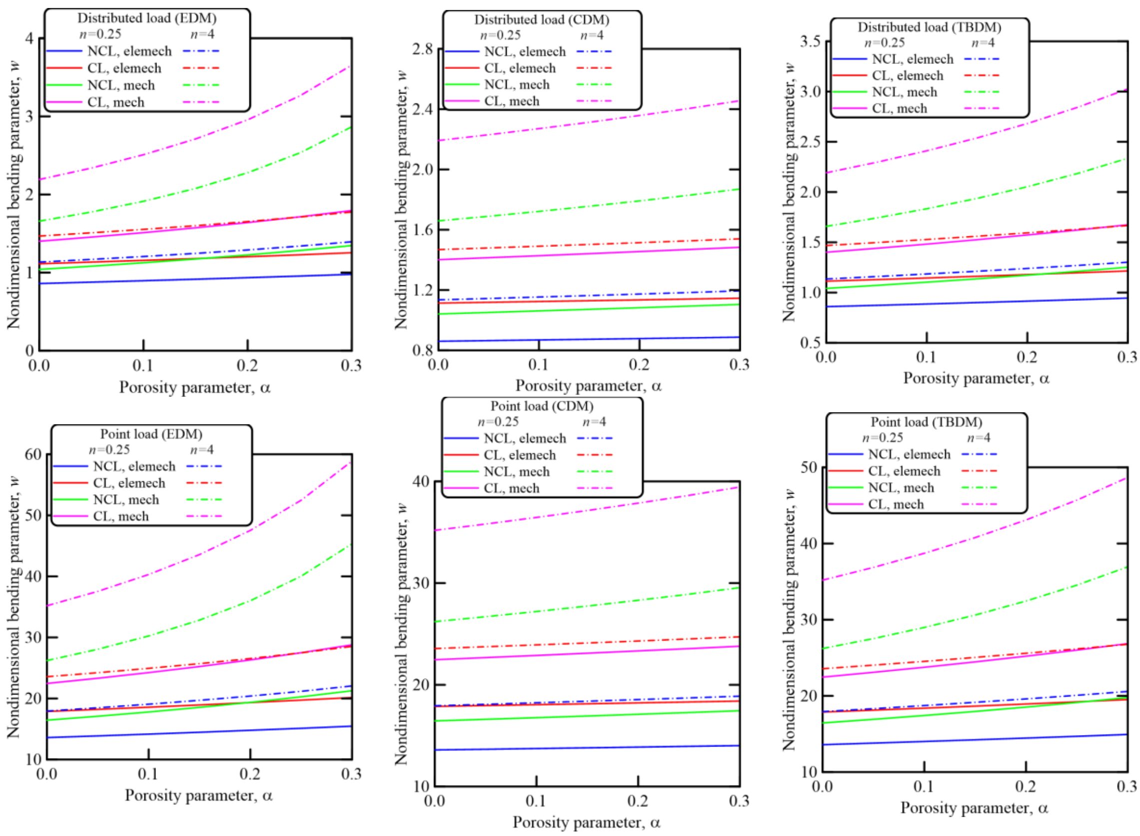

Fig. 2 Variation of the electromechanical and mechanical nondimensional bending parameter with the material porosity parameter, α at different values of the material gradation index, n for different porosity distribution models for uniformly distributed and central point loading conditions at beam slenderness ratio, L/h_t=20, K_p=2.5, K_w=5, e_0a/h_t=0.25, l/h_t=4, e_{311}=-4 C/m^2, μ_{3111}=5×10^{-8} C/m, and a_{33}=7.124×10^{-9} C/m^2 K

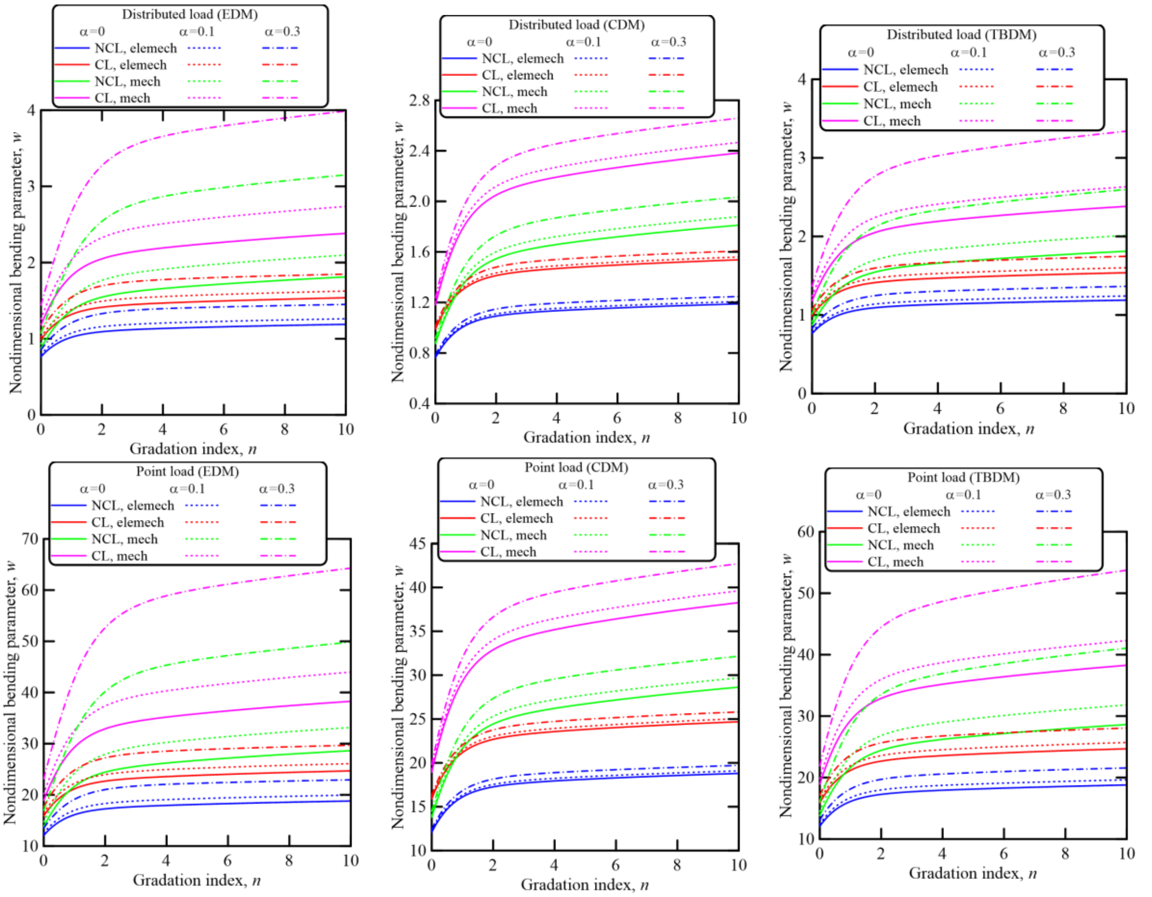

Fig. 3 Variation of the electromechanical and mechanical nondimensional bending parameter with the material gradation index, n at different values of the material porosity parameter, α for different porosity distribution models for uniformly distributed and central point loading conditions at beam slenderness ratio, L/h_t=20, K_p=2.5, K_w=5, e_0a/h_t=0.25, l/h_t=4, e_{311}=-4 C/m^2, μ_{3111}=5×10^{-8} C/m, and a_{33}=7.124×10^{-9} C/m^2 K

grading index produces larger values of the bending deflection parameters. Further, comparing the different material porosity models shows that the EDM results in larger drop in the overall system stiffness compared with CDM and TBDM models while the CDM porosity model produces smaller drop in the overall system stiffness. Furthermore, application of central concentrated load results in larger values of the bending deflection compared with the corresponding uniformly distributed loading cases.

6.2 Effect of the material grading index

Nonhomogeneity distribution of the functionally graded material characteristics through certain spatial coordinate has a significant impact on the bending behavior of nanobeam structures. To investigate the nonlinear relation between the bending deflection parameter and material grading index, the developed procedure is applied to detect the bending behavior over grading index interval [0,10]. Variation of the bending deflection parameters on the material gradation index for

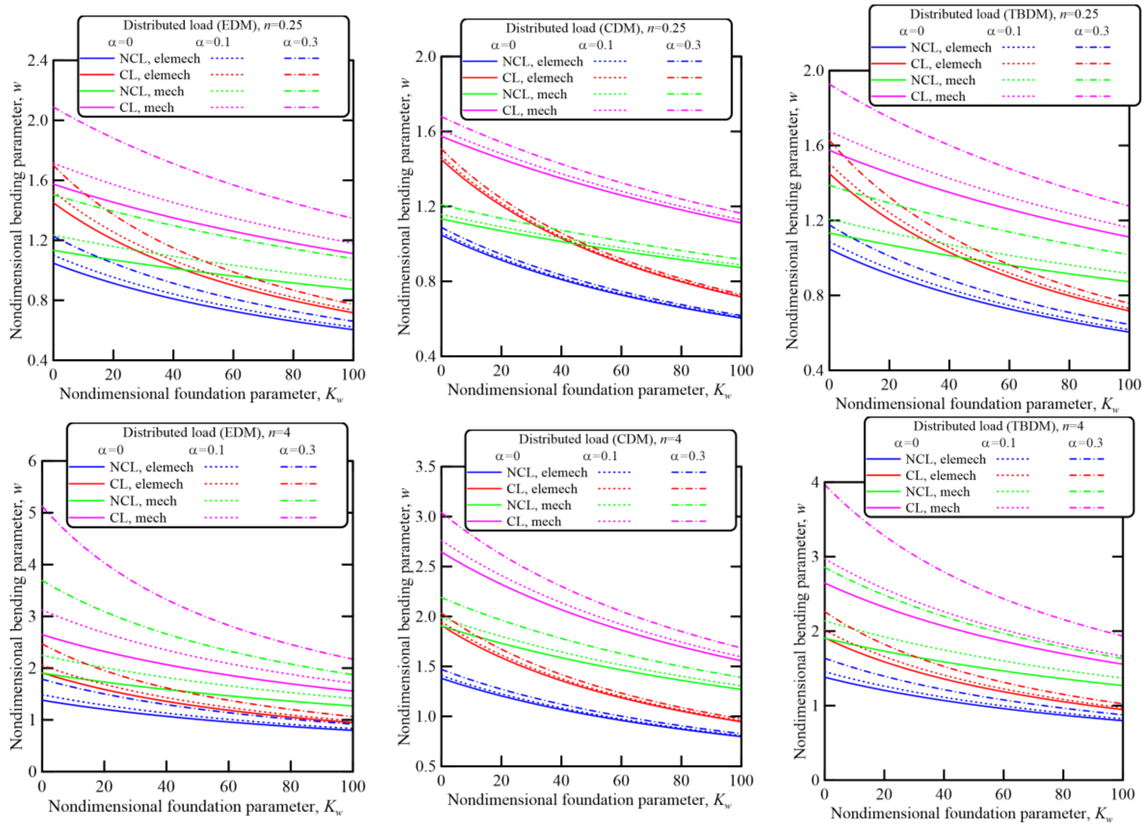

Fig. 4 Dependency of the electromechanical and mechanical nondimensional bending parameters of SS PFGNB under uniformly distributed load on the nondimensional elastic foundation parameter, K_w for nonclassical and classical analyses at different values of material gradation and porosity parameters for different porosity distribution models for L/h_t=20,n=0.25, 4, α=0, 0.1, 0.3, e_0a/h_t=0.25, l/h_t=4, e_{311}=-4 C/m^2, μ_{3111}=5×10^{-8} C/m, and a_{33}=7.124×10^{-9} C/m^{2}K

different material porosity distribution models at different values of material porosity parameter for both uniformly distributed and central point loading conditions is shown in Fig. 3. It may be seen that, according to the proposed material gradation, larger values of the maximum bending deflection parameters are produced by increasing the material grading index due to increasing the overall system flexibility for both electromechanical and mechanical behaviors. Additionally, incorporating the electrical effect leads to increasing the overall system stiffness which results in smaller values of the electromechanical bending deflection parameters compared with the corresponding mechanical parameters. Moreover, incorporating the size dependency effects significantly affects the static bending behavior, using larger values of the normalized size parameter, (l/h_t) over the normalized nonlocal parameters, (e_0a/h_t), (l/h)>(e_0a/h_t), leads to stiffening effect and produces smaller values of the nonclassical (*NCL*) normalized deflection parameters compared with the corresponding classical (*CL*) behavior. Furthermore, the applied loading condition significantly affects the detected bending deflection, it is noticed that the point loading condition produces larger values of the bending deflection parameters compared with the corresponding uniformly distributed load with the same equivalent load intensity.

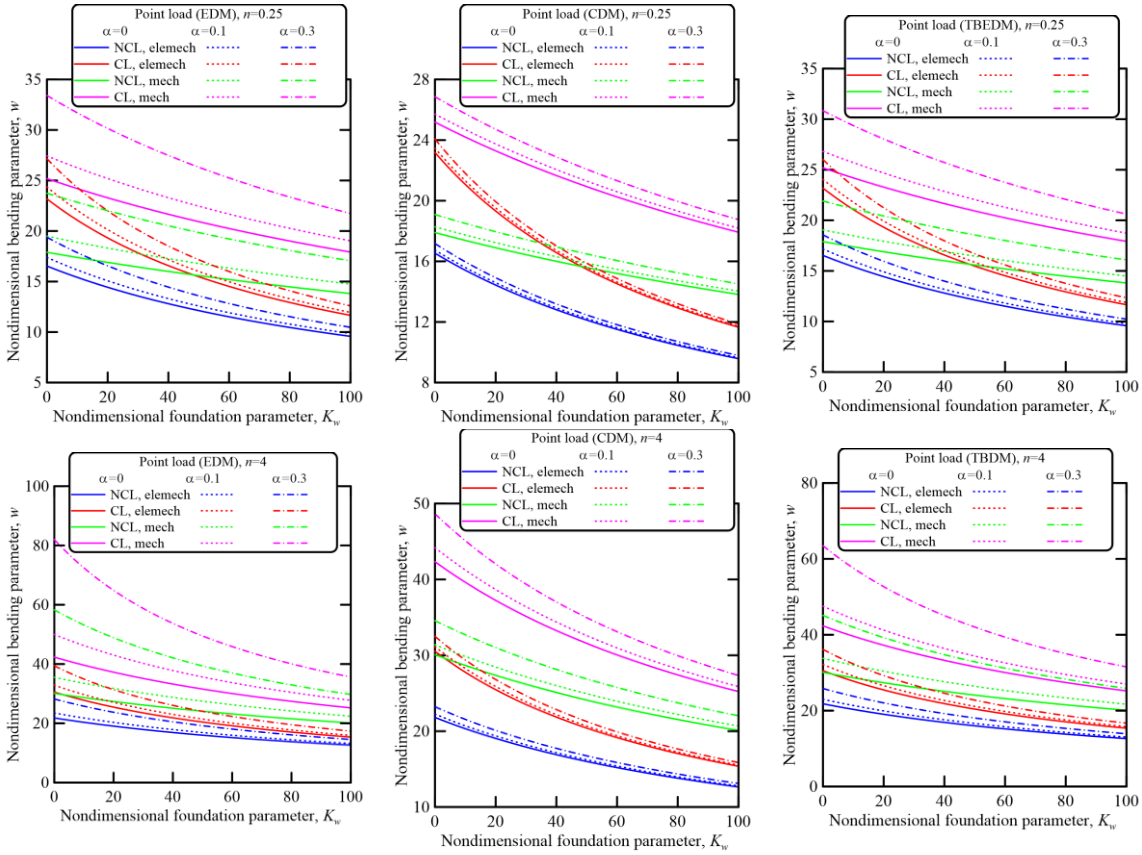

Fig. 5 variation of the electromechanical and mechanical nondimensional bending parameters of SS PFGNB under central point load with the nondimensional elastic foundation parameter, K_w for nonclassical and classical analyses at different values of material gradation and porosity parameters for different porosity distribution models L/h_t=20,n=0.25, 4, α=0, 0.1, 0.3, e_0a/h_t=0.25, l/h_t=4, e_{311}=-4 C/m^2, μ_{3111}=5×10^{-8} C/m, and a_{33}=7.124×10^{-9} C/m^{2}K

6.3 Effect of the Winkler-Pasternak elastic foundation parameters, K_w and K_p

The bending performance of the composite nanobeams embedded in an elastic environment could be controlled by controlling the parameters of this environment. The considered elastic environment is modeled as the Winkler-Pasternak elastic foundation. The bending deflection parameter dependency on the normalized elastic foundation parameters for porous functionally graded composite nanobeam layered with two identical piezoelectric layers are respectively depicted in Figs. 4-7. It is seen that the normalized bending deflection parameter is nonlinearly dependent on the elastic foundation parameters, K_w and K_p. Introduction of either Winkeler or Pasternak elastic environment parameters leads to increasing the overall system stiffness which results in nonlinear decaying of the normalized deflection parameters at all values of the material grading indices for both uniformly distributed and central point loads. Additionally, the Pasternak elastic foundation parameter has a more significant effect on the bending behavior. Larger

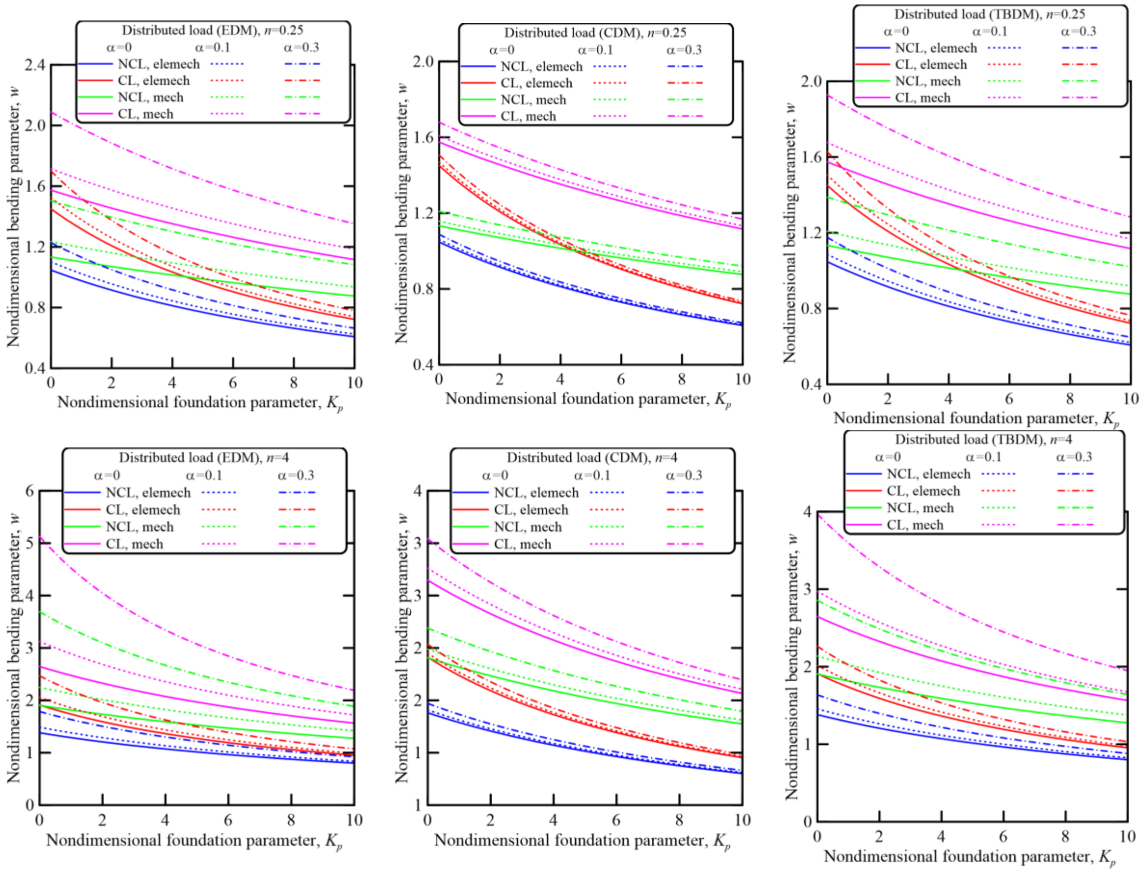

Fig. 6 Variation of the electromechanical and mechanical nondimensional bending parameters of SS PFGNB under uniformly distributed load with the nondimensional elastic foundation parameter, K_p for nonclassical and classical analyses at different values of material gradation and porosity parameters for different porosity distribution models for L/h_t=20, n=0.25, 4, α=0, 0.1,0.3, e_0a/h_t=0.25, l/h_t=4, e_{311}=-4 C/m^2, μ_{3111}=5×10^{-8} C/m, and a_{33}=7.124×10^{-9} C/m^{2}K

decrement in the normalized deflection parameters is obtained due to the Pasternak parameter, K_p compared with that of K_w.

Incorporating the material porosity effect significantly affects the bending behavior. Bending behavior is dependent on the porosity distribution and porosity parameter. Increasing the porosity parameter increases material flexibility and produces larger values of the bending deflection parameter. Additionally, the EDM porosity distribution model produces more flexible systems while the CDM porosity distribution profile results in less system flexibility compared with EDM and TBDM patterns. Further, introducing the nonlocal strain gradient effect with, (e_0a/h_t)=0.25 and (l/h_t=4), (l/h_t>e_0a/h_t) provides stiffening effect which produces smaller values of the normalized bending deflection parameters compared with the corresponding classical cases. Also, incorporating the piezoelectric as well as the flexoelectric effects provides more stiffening effects thus resulting in smaller values of the normalized electromechanical bending parameters compared with the corresponding mechanical cases. Furthermore, because of the Saint-Venant effect, application of central concentrated loads produces larger values of the electromechanical and the

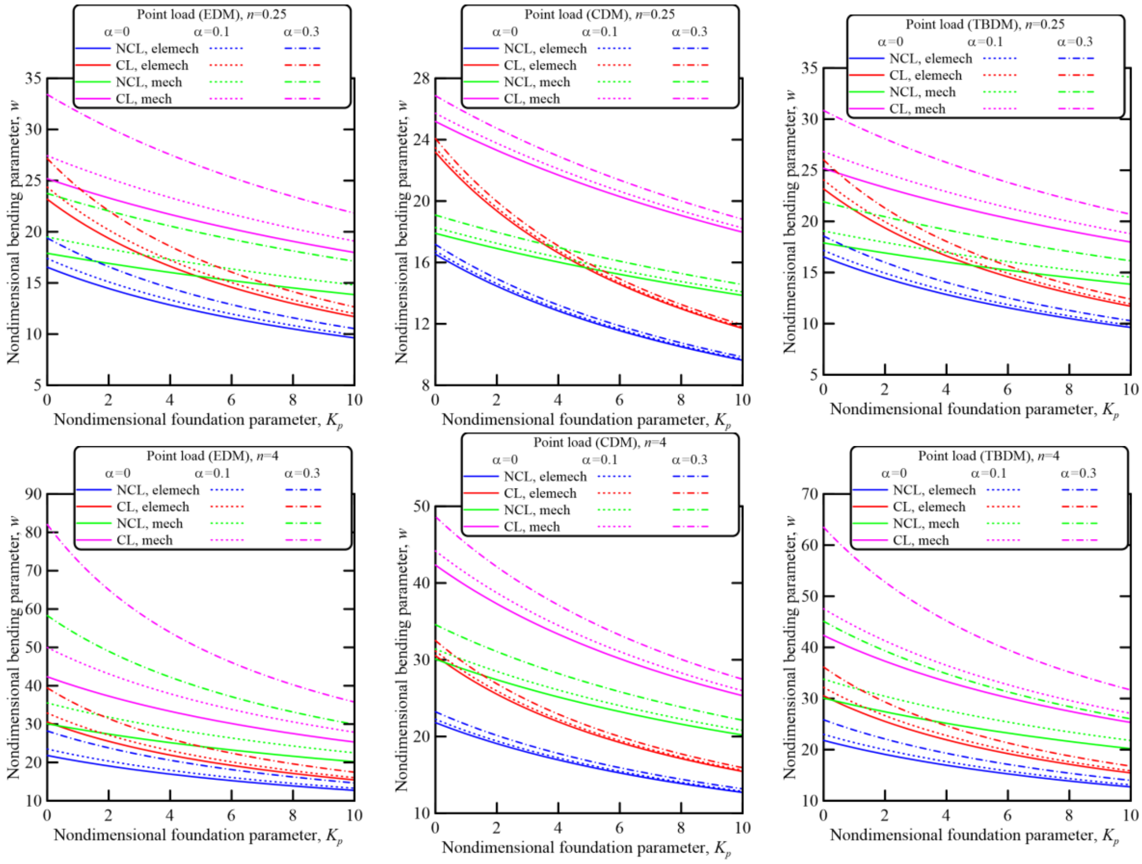

Fig. 7 Dependency of the electromechanical and mechanical nondimensional bending parameters of SS PFGNB central point load on the nondimensional elastic foundation parameter, K_p for nonclassical and classical analyses at different values of material gradation and porosity parameters for different porosity distribution models L/h_t=20,n=4, α=0, 0.1, 0.3, e_0a/h_t=0.25, l/h_t=4, e_{311}=-4 C/m^2, μ_{3111}=5×10^{-8} C/m, and a_{33}=7.124×10^{-9} C/m^{2}K

mechanical bending parameters compared to the corresponding uniformly distributed loading condition for nonclassical and classical behaviors.

6.4 Effect of the normalized size parameter (l/h_t)

Influence of the normalized size parameter, (l/h_t) on the size dependent electromechanical as well as mechanical behaviors for different porosity models at different values of the material grading and porosity indices for uniformly distributed and concentrated loads is depicted in Fig. 8**.** It may be indicated that the nonclassical bending deflection parameters are nonlinearly decayed with increasing the normalized strain gradient parameter, (l/h_t) for both electromechanical and mechanical behaviors. Additionally, increasing the material grading index increases the overall system flexibility due to increasing the material metal content thus larger values of the bending deflection parameters are detected. On the other hand, increasing the material porosity parameter also reduces the overall system stiffness this increases the bending deflection parameters.

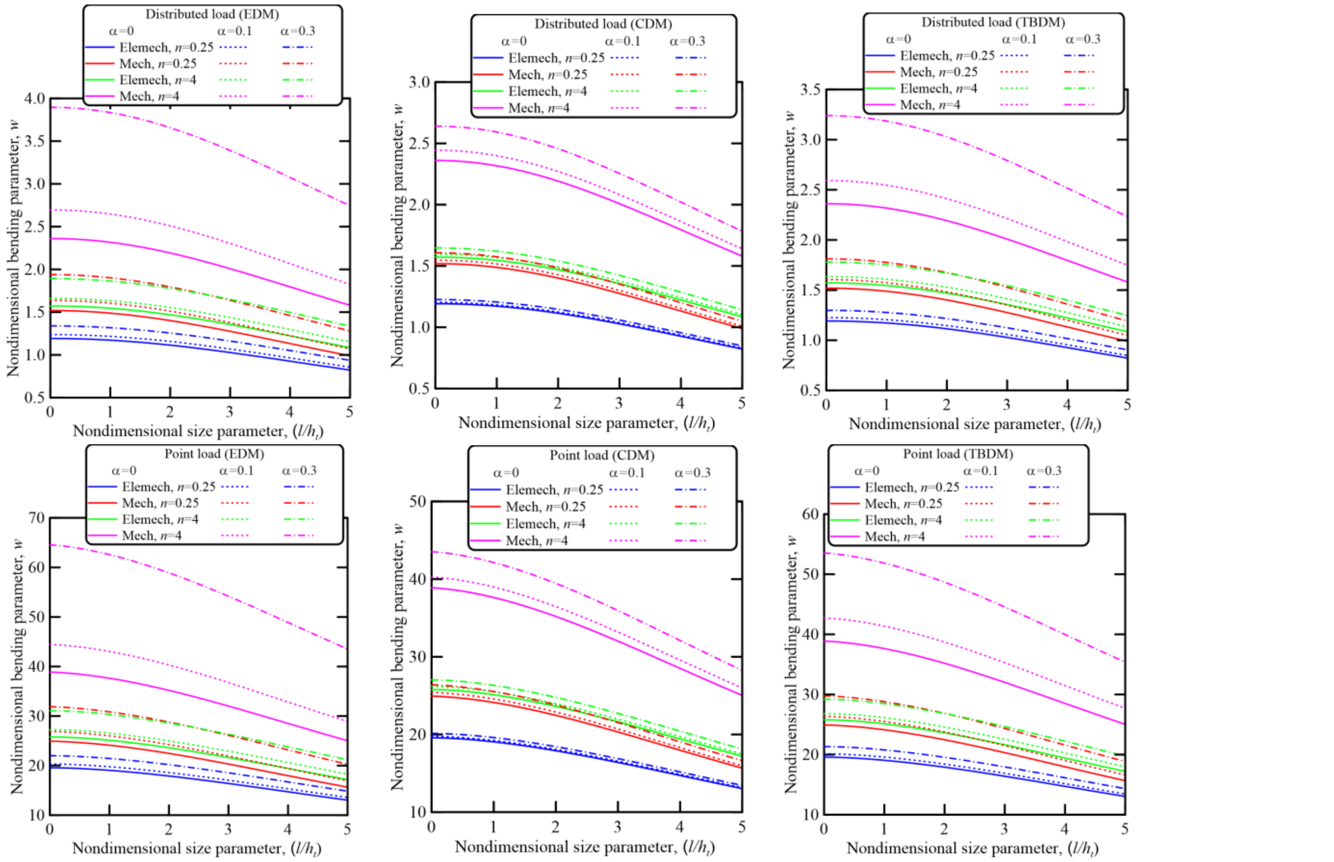

Fig. 8 Variation of the size dependent electromechanical and mechanical nondimensional bending parameter of SS nanobeam with the nondimensional size parameter, l/h_t, at different values of material gradation, porosity parameters and porosity distribution models for uniformly distributed and point loads for n=0.25, 4, α=0, 0.1, 0.3, e_0a/h_t=2, L/h_t=20, K_w=5, K_p=2.5, e_{311}=-4C/m^2, μ_{3111}=5×10^{-8}C/m, and a_{33}=7.124×10^{-9} C/m^{2}K

6.5 Effect of the normalized nonlocal parameter (e_0a/h_t)

Impact of the normalized nonlocal parameter, (e_0a/h_t) on the size dependent bending deflection for electromechanical as well as mechanical behaviors at different values of material grading and porosity parameters for different porosity distribution profiles are depicted in Fig. 9. It is noticed that the nonclassical bending deflection parameters are nonlinearly dependent on the normalized nonlocal parameter. Due to the associated softening effect with increasing(e_0a/h_t), larger values of the normalized bending deflection parameters are detected for electromechanical as well as mechanical behaviors. Additionally, flexibility effect is provided by increasing the material grading index, n as well as the material porosity parameter, α due to reduction of the overall system stiffness.

6.6 Effect of the electric field-strain gradient coupling coefficient, (μ_{3111})

Keeping constant value of the piezoelectric coefficient, e_{311}, the influence of electric field-strain

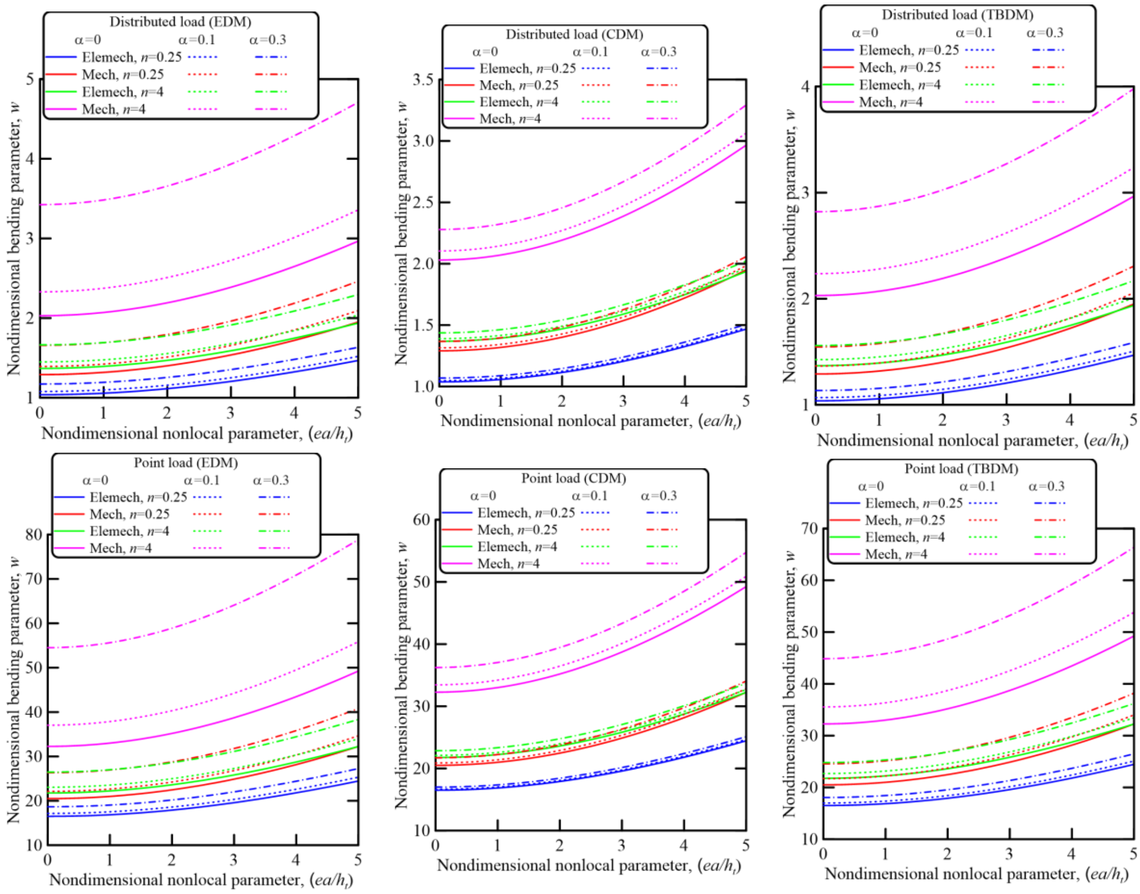

Fig. 9 Variation of the nonclassical electromechanical and mechanical nondimensional bending parameter of SS nanobeam with the normalized nonlocal parameter, ea/h_t, at different values of material gradation, porosity parameters and porosity distribution models for uniformly distributed and point loads for n=0.25, 4, α=0, 0.1, 0.3, e_0a/h_t=2, L/h_t=20, and K_w=5, K_p=2.5, e_{311}=-4C/m^2, μ_{3111}=5×10^{-8}C/m, and a_{33}=7.124×10^{-9} C/m^{2}K

gradient coupling coefficient, μ_{3111} on the size dependent and classical electromechanical bending behaviors of piezoelectric composite FG nanobeams for different porosity distribution models at different values of material grading and porosity parameters is detected for interval [-5,5] ×10^{-8} in Fig. 10. It may be observed that, according to the material and geometrical characteristics, the electromechanical normalized bending deflection is nonlinearly dependent on the electric field-strain gradient coupling coefficient. The normalized bending deflection is decreased by increasing the absolute value of μ_{3111} for classical and nonclassical behaviors at all values of material gradation and porosity parameters. Further, an increase in the normalized bending deflection is detected with increasing the material gradation and porosity indices due to decreasing the overall system stiffness. Additionally, the porosity distribution significantly affects the bending behavior, EDM results in more system flexibility while CDM leads to low system flexibility. Also, application of concentrated load results in larger values of bending deflection compared with the corresponding cases of uniformly distributed load.

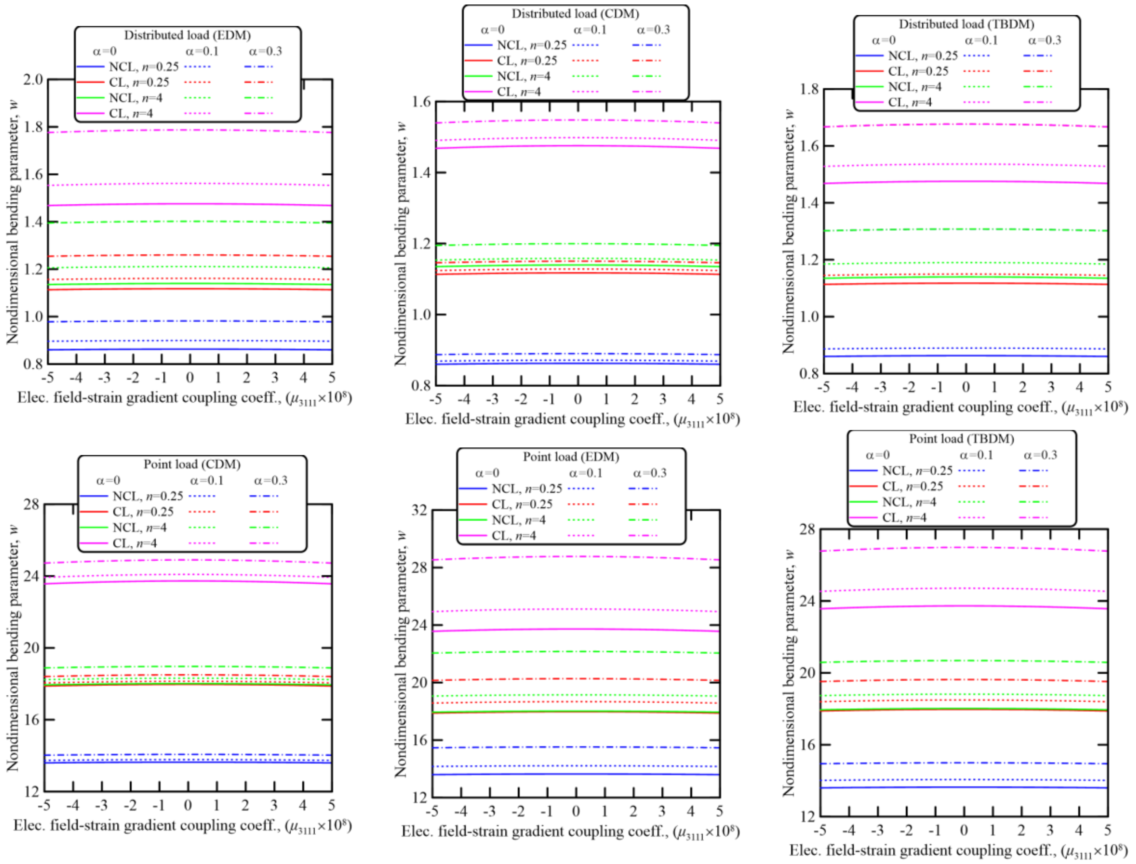

Fig 10 Dependency of the classical and nonclassical electromechanical normalized bending parameter of SS nanobeam on the electric field-strain gradient coupling coefficient, μ_{3111}, at different values of material gradation, porosity parameters and porosity distribution models for uniformly distributed and point loads at n=0.25, 4, α=0, 0.1, 0.3, l_c/h_t=4, e_0a/h_t=0.25, L/h=20, K_p=2.5, K_w=5, e_{311}=-4C/m^2, and a_{33}=7.124×10^{-9} C/m^{2}K

6.7 Effect of the piezoelectric coefficient, (e_{311})

To demonstrate the impact of the piezoelectric coefficient, e_{311} on the electromechanical bending deflection behavior of piezoelectric porous functionally graded composite nanobeams embedded in an elastic environment at constant value of the electric field-strain gradient coupling coefficient, μ_{3111}, dependency of the electromechanical bending behavior is detected over e_{311} interval [-5,5], as illustrated in Fig. 11. As stated previously for the impact of the electric field-strain gradient coupling coefficient, μ_{3111}, the electromechanical bending parameter is also nonlinearly dependent on the piezoelectric coefficient. The electromechanical bending deflection parameters decay with increasing the absolute value of the piezoelectric coefficient due to the associated stiffening effect. Additionally, increasing material grading or porosity parameters results in more system flexibility thus produces larger values of the normalized bending parameters for both size dependent and classical behaviors.

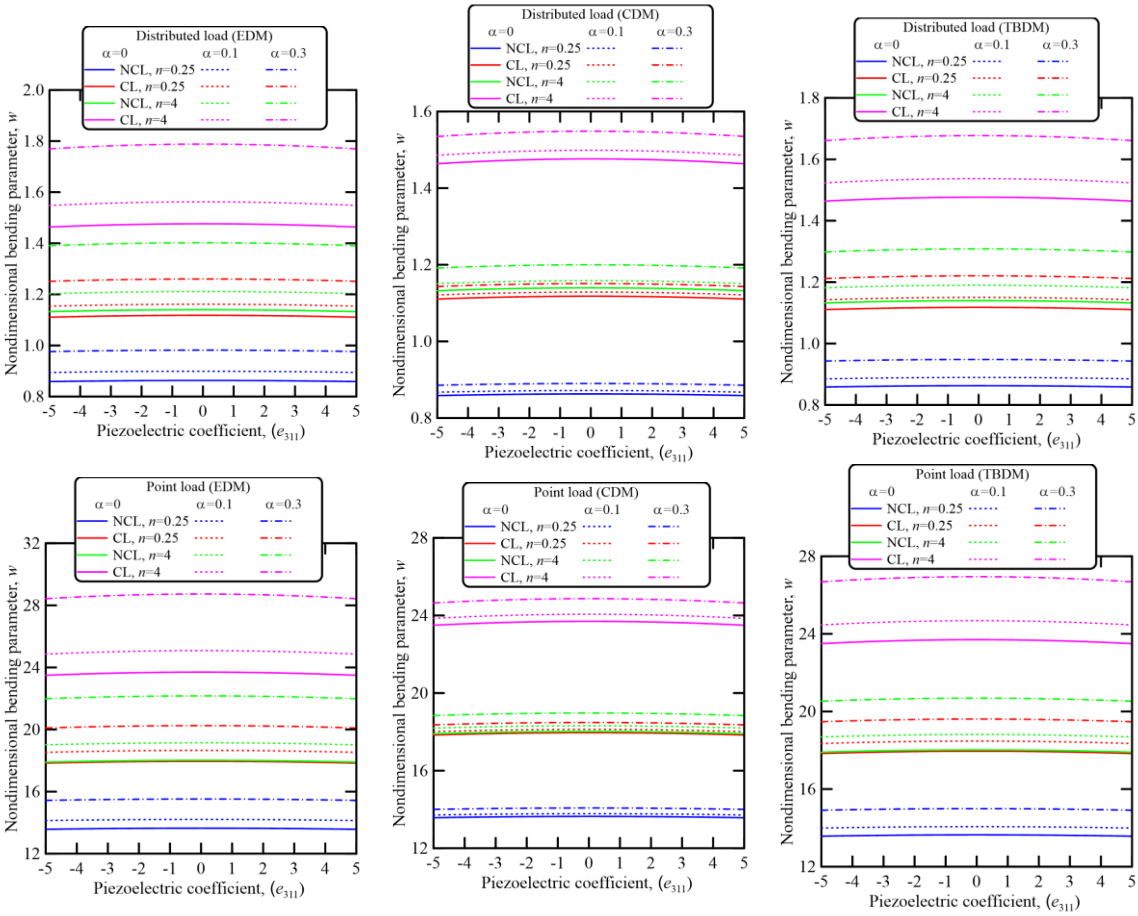

Fig. 11 Dependency of the classical and nonclassical electromechanical normalized bending parameter of SS nanobeam on the piezoelectric coefficient, e_{311}, at different values of material gradation, porosity parameters and porosity distribution models for uniformly distributed and point loads at n=0.25, 4, α=0, 0.1, 0.3, l_c/h_t=4, e_0a/h_t=0.25, L/h=20, K_p=2.5, K_w=5, μ_{3111}=5×10^{-8}C/m, and a_{33}=7.124×10^{-9} C/m^{2}K

7. Conclusions

In the frameworks of modified nonlocal strain gradient theory, the size-dependent bending performance of a piezoelectrically layered composite nanobeam with a porous functionally graded core, resting on an elastic foundation, and incorporating flexoelectricity is investigated and analyzed. Key findings include:

• Porosity distribution patterns and porosity indicator have a significant impact on the bending performance of piezoelectric composite nanobeams with piezoelectric layers. This performance could be enhanced by controlling the porosity indicator and the porosity distribution configuration.

• The porosity distribution profiles significantly affect the bending performance of piezoelectrically layered composite nanobeams with porous functionally graded core. The CDM porosity distribution pattern provides less system flexibility thus producing smaller values of the bending deflection parameters compared with EDM and TBDM porosity distribution profiles. On the other hand, EDM porosity distribution model results in more system flexibility compared with CDM and TBDM models.

• The porosity indicator has a significant influence on the bending behavior of pours functionally graded composite nanobeams layered with piezoelectric layers. Growing up this indicator provides more system flexibility leading to producing larger values of the bending deflection parameters.

• The material distribution and gradation significantly influence the bending behavior. Increasing the metal content in the porous functionally graded core leads to greater flexibility and larger bending deflections.

• The elastic foundation provides additional support to the nanobeam, reducing its deflection and stress.

• The modified nonlocal strain gradient theory effectively captures the size-dependent behavior of the nanobeam, leading to significant deviations from classical elasticity theory. Both stiffening and softening effects can be provided by controlling the sized and nonlocality parameters.

• The flexoelectric effect plays a crucial role in the electromechanical coupling of the nanobeam, influencing its bending response.

• The applied loading profile significantly affects the detected bending behavior. Point loading conditions result in larger bending deflections compared to uniformly distributed loads.

• The proposed model and the developed analytical solution strategy provide valuable insights for the design and optimization of nanobeam-based devices, such as sensors, actuators, and energy harvesters.

References

Abdelrahman, A.A. and Eltaher, M.A. (2022), "On bending and buckling responses of perforated nanobeams including surface energy for different beams theories", *Eng. Comput.*, **38**(3), 2385-2411. https://doi.org/10.1007/s00366-020-01211-8.

Abdelrahman, A.A., Abdel-Mottaleb, H.E., Aljabri, A., Mahmoud, E.R. and Eltaher, M.A. (2024a), "Modeling of size dependent buckling behavior of piezoelectric sandwich perforated nanobeams rested on elastic foundation with flexoelectricity", *Mech. Bas. Des. Struct. Mach.*, 1-27. https://doi.org/10.1080/15397734.2024.2365918.

Abdelrahman, A.A., Abd-El-Mottaleb, H.E., Elblassy, M.G. and Elshamy, E.A. (2023a), "Vibrations and stress analysis of perforated functionally graded rotating beams", *Steel Compos. Struct.*, **49**(6), 667-684. https://doi.org/10.12989/scs.2023.49.6.667.

Abdelrahman, A.A., Abdelwahed, M.S., Ahmed, H.M., Hamdi, A. and Eltaher, M.A. (2023b), "Investigation of size-dependent vibration behavior of piezoelectric composite nanobeams embedded in an elastic foundation considering flexoelectricity effects", *Math.*, **11**(5), 1180. https://doi.org/10.3390/math11051180.

Abdelrahman, A.A., Ashry, M., Alshorbagy, A.E. and Abdallah, W.S. (2021), "On the mechanical behavior of two directional symmetrical functionally graded beams under moving load", *Int. J. Mech. Mater. Des.*, **17**, 563-586. https://doi.org/10.1007/s10999-021-09547-9.

Abdelrahman, A.A., Ashry, M., Alshorbagy, A.E., Eltaher, M.A. and Abdalla, W.S. (2024b), "On the dynamic behavior of functionally graded cracked beams resting on Winkler foundation under moving load", *Steel Compos. Struct.*, **53**(2), 169-194. https://doi.org/10.12989/scs.2024.53.2.169.

Abdelrahman, A.A., El-Shafei, A.G. and Mahmoud, F.F. (2014), "Nonlinear analysis of viscoelastically layered rolls in steady state rolling contact", *Int. J. Appl. Mech.*, **6**(06), 1450065. https://doi.org/10.1142/S1758825114500653.

Abdelrahman, A.A., Saleem, H.A., Abdelhaffez, G.S. and Eltaher, M.A. (2023c), "On bending of piezoelectrically layered perforated nanobeams embedded in an elastic foundation with flexoelectricity", *Math.*, **11**(5), 1162. https://doi.org/10.3390/math11051162.

Ait Atmane, H., Tounsi, A. and Bernard, F. (2017), "Effect of thickness stretching and porosity on mechanical response of a functionally graded beams resting on elastic foundations", *Int. J. Mech. Mater. Des.*, **13**, 71-84. https://doi.org/10.1007/s10999-015-9318-x.

Alasadi, A.A., Ahmed, R.A. and Faleh, N.M. (2019), "Analyzing nonlinear vibrations of metal foam nanobeams with symmetric and non-symmetric porosities", *Adv. Aircraft Spacecraft Sci.*, **6**(4), 273-282. https://doi.org/10.12989/aas.2019.6.4.273.

Alazwari, M.A., Eltaher, M.A. and Abdelrahman, A.A. (2022), "On bending of cutout nanobeams based on nonlocal strain gradient elasticity theory", *Steel Compos. Struct.*, **43**(6), 707-723. https://doi.org/10.12989/scs.2022.43.6.707.

Alessi, Y.A., Ali, I., Alazwari, M.A., Almitani, K., Abdelrahman, A.A. and Eltaher, M.A. (2023). Dynamic analysis of piezoelectric perforated cantilever bimorph energy harvester via finite element analysis", *Adv. Aircraft Spacecraft Sci.*, **10**(2), 179. https://doi.org/10.12989/aas.2023.10.2.179.

Al-Furjan, M.S.H., Kong, X.S., Shan, L., Soleimani Jafari, G., Farrokhian, A., Shen, X., Kolahchi, R. and Rajak, D.K. (2022), "Influence of LPRE on the size-dependent phase velocity of sandwich beam including FG porous and smart nanocomposite layers", *Polym. Compos.*, **43**(10), 7390-7402. https://doi.org/10.1002/pc.26820.

Ali, I.A., Alazwari, M.A., Eltaher, M.A. and Abdelrahman, A.A. (2022), "Effects of viscoelastic bonding layer on performance of piezoelectric actuator attached to elastic structure", *Mater. Res. Expr.*, **9**(4), 045701. https://doi.org/10.1088/2053-1591/ac5cae.

Almitani, K.H., Eltaher, M.A., Abdelrahman, A.A. and Abd-El-Mottaleb, H.E. (2021), "Finite element based stress and vibration analysis of axially functionally graded rotating beams", *Struct. Eng. Mech.*, **79**(1), 23-33. https://doi.org/10.12989/sem.2021.79.1.023.

Alnujaie, A., Abdelrahman, A.A., Alanasari, A.M. and Eltaher, M.A. (2023), "Influence of flexoelectricity on bending of piezoelectric perforated FG composite nanobeam rested on elastic foundation", *Steel Compos. Struct.*, **49**(4), 361-380. https://doi.org/10.12989/scs.2023.49.4.361.

Alshenawy, R., Sahmani, S., Safaei, B., Elmoghazy, Y., Al-Alwan, A. and Sobhy, M. (2023), "Nonlinear dynamical performance of microsize piezoelectric bridge-type energy harvesters based upon strain gradient-based meshless collocation approach", *Eng. Anal. Bound. Elem.*, **151**, 199-215. https://doi.org/10.1016/j.enganabound.2023.03.002.

Ansari, R., Nesarhosseini, S., Faraji Oskouie, M. and Rouhi, H. (2021), "Size-dependent buckling analysis of piezoelectric nanobeams resting on elastic foundation considering flexoelectricity effect using the stress-driven nonlocal model", *Eur. Phys. J. Plus*, **136**-876. https://doi.org/10.1140/epjp/s13360-021-01837-7.

Assie, A., Mohamed, S., Abdelrahman, A.A. and Eltaher, M.A. (2023), "Mathematical formulations for static behavior of bi-directional FG porous plates rested on elastic foundation including middle/neutral-surfaces", *Steel Compos. Struct.*, **48**(2), 113-130. https://doi.org/10.12989/scs.2023.48.2.113.

Attia, M.A. and Abdelrahman, A.A. (2018), "On vibrations of functionally graded viscoelastic nanobeams with surface effects", *Int. J. Eng. Sci.*, **127**, 1-32. https://doi.org/10.1016/j.ijengsci.2018.02.005.

Basha, M., Daikh, A.A., Melaibari, A., Wagih, A., Othman, R., Almitani, K.H., ... & Eltaher, M.A. (2022), "Nonlocal strain gradient theory for buckling and bending of FG-GRNC laminated sandwich plates", *Steel Compos. Struct.*, **43**(5), 639-660. https://doi.org/10.12989/scs.2022.43.5.639.

Chen, W.Q., Lü, C.F. and Bian, Z.G. (2004), "A mixed method for bending and free vibration of beams resting on a Pasternak elastic foundation", *Appl. Math. Model.*, **28**(10), 877-890. https://doi.org/10.1016/j.apm.2004.04.001

Chu, L., Dui, G. and Ju, C. (2018), "Flexoelectric effect on the bending and vibration responses of functionally graded piezoelectric nanobeams based on general modified strain gradient theory", *Compos.*

Struct., **186**, 39-49. https://doi.org/10.1016/j.compstruct.2017.10.083.

Dang, V.H. and Do, Q.C. (2021), "Nonlinear vibration and stability of functionally graded porous microbeam under electrostatic actuation", *Arch. Appl. Mech.*, **91**(5), 2301-2329. https://doi.org/10.1007/s00419-021-01884-7.

Ebrahimi, F. and Hosseini, S.H.S. (2020), "Resonance analysis on nonlinear vibration of piezoelectric/FG porous nanocomposite subjected to moving load", *Eur. Phys. J. Plus*, **135**(2), 1-23. https://doi.org/10.1140/epjp/s13360-019-00011-4.

Eftekhari, S.A. and Toghraie, D. (2022), "Vibration and dynamic analysis of a cantilever sandwich microbeam integrated with piezoelectric layers based on strain gradient theory and surface effects", *Appl. Math. Comput.*, **419**, 126867. https://doi.org/10.1016/j.amc.2021.126867.

Eltaher, M.A., Abdelmoteleb, H.E., Daikh, A.A. and Abdelrahman, A.A. (2021), "Vibrations and stress analysis of rotating perforated beams by using finite elements method", *Steel Compos. Struct.*, **41**(4), 505-520. https://doi.org/10.12989/scs.2021.41.4.505.

Eltaher, M.A., Abdelrahman, A.A., Al-Nabawy, A., Khater, M. and Mansour, A. (2014), "Vibration of nonlinear graduation of nano-Timoshenko beam considering the neutral axis position", *Appl. Math. Comput.*, **235**, 512-529. https://doi.org/10.1016/j.amc.2014.03.028.

Esen, I., Alazwari, M.A., Almitani, K.H., Eltaher, M.A. and Abdelrahman, A. (2023), "Dynamic vibration response of functionally graded porous nanoplates in thermal and magnetic fields under moving load. *Adv. Nano Res.*, **14**(5), 475. https://doi.org/10.12989/anr.2023.14.5.475.

Esen, I., Alazwari, M.A., Eltaher, M.A. and Abdelrahman, A.A. (2022), "Dynamic response of FG porous nanobeams subjected thermal and magnetic fields under moving load", *Steel Compos. Struct.*, **42**(6), 805-826. https://doi.org/10.12989/scs.2022.42.6.805.

Fahsi, B., Bouiadjra, R.B., Mahmoudi, A., Benyoucef, S. and Tounsi, A. (2019), "Assessing the effects of porosity on the bending, buckling, and vibrations of functionally graded beams resting on an elastic foundation by using a new refined quasi-3D theory", *Mech. Compos. Mater.*, **55**(2), 219-230. https://doi.org/10.1007/s11029-019-09805-0.

Hosseini, S.A.H., Moghaddam, M.H. and Rahmani, O. (2020), "Exact solution for axial vibration of the power, exponential and sigmoid FG nonlocal nanobeam", *Adv. Aircraft Spacecraft Sci.*, **7**(6), 517-536. https://doi.org/10.12989/aas.2020.7.6.517

Hosseini-Hashemi, S., Nahas, I., Fakher, M. and Nazemnezhad, R. (2014), "Surface effects on free vibration of piezoelectric functionally graded nanobeams using nonlocal elasticity", *Acta Mechanica*, **225**, 1555-1564. https://doi.org/10.1007/s00707-013-1014-z.

HS, N.K. (2022), "Geometrically Nonlinear Vibration Analysis of Functionally Graded Porous Plates and Shells", Doctoral Dissertation, National Institute of Technology Karnataka, Surathkal.

Liang, X., Hu, S.L. and Shen, S.P. (2014), "Effects of surface and flexoelectricity on a piezoelectric nanobeam", *Smart Mater. Struct.*, **23**(3), 035020. https://doi.org/10.1088/0964-1726/23/3/035020.

Lu, L., Guo, X. and Zhao, J. (2017), "A unified nonlocal strain gradient model for nanobeams and the importance of higher order terms", *Int. J. Eng. Sci.*, **119**, 265-277. http://doi.org/10.1016/j.ijengsci.2017.06.024.

Mehralian, F., Beni, Y.T. and Zeverdejani, M.K. (2017), "Nonlocal strain gradient theory calibration using molecular dynamics simulation based on small scale vibration of nanotubes", *Physica B: Condens. Mat.*, **514**, 61-69. https://doi.org/10.1016/j.physb.2017.03.030.

Melaibari, A., Abdelrahman, A.A., Hamed, M.A., Abdalla, A.W. and Eltaher, M.A. (2022), "Dynamic analysis of a piezoelectrically layered perforated nonlocal strain gradient nanobeam with flexoelectricity", *Math.*, **10**(15), 2614. https://doi.org/10.3390/math10152614.

Mirjavadi, S.S., Mohasel Afshari, B., Khezel, M., Shafiei, N., Rabby, S. and Kordnejad, M. (2018), "Nonlinear vibration and buckling of functionally graded porous nanoscaled beams", *J. Brazil. Soc. Mech. Sci. Eng.*, **40**, 1-12. https://doi.org/10.1007/s40430-018-1272-8.

Mohamed, N., Mohamed, S.A. and Eltaher, M.A. (2024), "Exact solutions of vibration and postbuckling response of curved beam rested on nonlinear viscoelastic foundations", *Adv. Aircraft Spacecraft Sci.*, **11**(1), 55-81. https://doi.org/10.12989/aas.2024.11.1.055

Mohamed, N.A., Shanab, R.A., Eltaher, M.A. and Abdelrahman, A.A. (2024), "Vibration response of viscoelastic perforated higher-order nanobeams rested on an elastic substrate under moving load", *Acta Mechanica*, **235**(2), 1213-1233. https://doi.org/10.1007/s00707-023-03776-z.

Nabawy, A.E., Abdelhaleem, A.M., Ali-Eldin, S.S. and Abdelrahman, A.A. (2022), "Study of the dynamic behavior of porous functionally graded suspension structural systems using finite elements method", *Steel Compos. Struct.*, **45**(5), 697-713. https://doi.org/10.12989/scs.2022.45.5.697.

Nan, Z., Xie, Z., Shijie, Z. and Dejin, C. (2020), "Size-dependent static bending and free vibration analysis of porous functionally graded piezoelectric nanobeams", *Smart Mater. Struct.*, **29**(4), 045025. https://doi.org/10.1088/1361-665X/ab73e4.

Rahmani, F., Kamgar, R. and Rahgozar, R. (2020), "Finite element analysis of functionally graded beams using different beam theories", *Civil Eng. J.*, **6**(11), 2086-2102. http://doi.org/10.28991/cej-2020-03091604.

Ren, Y.M., Schiavone, P. and Qing, H. (2022), "On well-posed integral nonlocal gradient piezoelectric models for static bending of functionally graded piezoelectric nanobeam", *Eur. J. Mech.-A/Solid.*, **96**, 104735. https://doi.org/10.1016/j.euromechsol.2022.104735.

Selvamani, R., Rexy, J.B. and Ebrahimi, F. (2022), "Finite element modeling and analysis of piezoelectric nanoporous metal foam nanobeam under hygro and nonlinear thermal field", *Acta Mechanica*, **233**(8), 3113-3132. https://doi.org/10.1007/s00707-022-03263-x

Siam, O.A., Shanab, R.A., Eltaher, M.A. and Mohamed, N.A. (2023), "Free vibration analysis of nonlocal viscoelastic nanobeam with holes and elastic foundations by Navier analytical method", *Adv. Aircraft Spacecraft Sci.*, **10**(3), 257-279. https://doi.org/10.12989/aas.2023.10.3.257

Şimşek, M. and Yurtcu, H.H. (2013), "Analytical solutions for bending and buckling of functionally graded nanobeams based on the nonlocal Timoshenko beam theory", *Compos. Struct.*, **97**, 378-386. http://dx.doi.org/10.1016/j.compstruct.2012.10.038.

Tadi Beni, Y. (2016), "Size-dependent electromechanical bending, buckling, and free vibration analysis of functionally graded piezoelectric nanobeams", *J. Intel. Mater. Syst. Struct.*, **27**(16), 2199-2215. https://doi.org/10.1177/1045389X15624798.

Thongchom, C., Saffari, P.R., Refahati, N., Saffari, P.R., Pourbashash, H., Sirimontree, S. and Keawsawasvong, S. (2022), "An analytical study of sound transmission loss of functionally graded sandwich cylindrical nanoshell integrated with piezoelectric layers", *Scientif. Report.*, **12**(1), 3048. https://doi.org/10.1038/s41598-022-06905-1.

Van Minh, P., Thai, L.M., Dung, N.T., Tounsi, A., Nhung, N.T.C. and Van Thom, D. (2023), "An overview of the flexoelectric phenomenon, potential applications, and proposals for further research directions", *Int. J. Mech. Mater. Des.*, **19**(4), 903-925. https://doi.org/10.1007/s10999-023-09678-1.

Wang, X. and Xue, Y. (2023), "Investigation of the electric response of the piezoelectric curved beam considering the direct piezoelectric and flexoelectric effects", *Thin Wall. Struct.*, **188**, 110839. https://doi.org/10.1016/j.tws.2023.110839.

Wattanasakulpong, N. and Chaikittiratana, A. (2015), "Flexural vibration of imperfect functionally graded beams based on Timoshenko beam theory: Chebyshev collocation method", *Meccanica*, **50**, 1331-1342. https://doi.org/10.1007/s11012-014-0094-8.

Yadav, S.S., Sangle, K.K., Kokane, M.U., Pendhari, S.S. and Ghugal, Y.M. (2023), "Bending analysis of exponentially varied FG plates using trigonometric shear and normal deformation theory", *Adv. Aircraft Spacecraft Sci.*, **10**(3), 281. https://doi.org/10.12989/aas.2023.10.3.281

Yan, Z. and Jiang, L. (2017), "Modified continuum mechanics modeling on size-dependent properties of piezoelectric nanomaterials: A review", *Nanomater.*, **7**(2), 27. https://doi.org/10.3390/nano7020027.

Ying, J., Lu, C.F. and Chen, W.Q. (2008), "Two-dimensional elasticity solutions for functionally graded beams resting on elastic foundations", *Compos. Struct.*, **84**, 209-219. https://doi.org/10.1016/j.compstruct.2007.07.004

Zeng, S., Wang, K., Wang, B. and Wu, J. (2020), "Vibration analysis of piezoelectric sandwich nanobeam with flexoelectricity based on nonlocal strain gradient theory", *Appl. Math. Mech.*, **41**(6), 859-880. https://doi.org/10.1007/s10483-020-2620-8.

Zhang, N., Zheng, S. and Chen, D. (2022), "Size-dependent static bending, free vibration and buckling analysis of curved flexomagnetic nanobeams", *Meccanica*, **57**(7), 1505-1518. https://doi.org/10.1007/s11012-022-01506-8.

Zhao, X., Zheng, S. and Chen, D. (2023), "Size-dependent nonlinear analysis of piezo-electrostatically actuated porous functionally graded nanobeams incorporating flexoelectricity", *J. Brazil. Soc. Mech. Sci. Eng.*, **45**(2), 97. https://doi.org/10.1007/s40430-022-03983-0.

Zhao, X., Zheng, S. and Li, Z. (2020), "Effects of porosity and flexoelectricity on static bending and free vibration of AFG piezoelectric nanobeams", *Thin Wall. Struct.*, **151**, 106754. https://doi.org/10.1016/j.tws.2020.106754.

Zhao, X., Zheng, S. and Li, Z. (2022), "Bending, free vibration and buckling analyses of AFG flexoelectric nanobeams based on the strain gradient theory", *Mech. Adv. Mater. Struct.*, **29**(4), 548-563. https://doi.org/10.1080/15376494.2020.1779880.

Zheng, S., Zhang, N., Zhao, X., Chen, D. and Wang, H.T. (2024), "Size-dependent mechanical analysis of porous functionally graded piezoelectric micro/nanoscale structures: A literature review", *Smart Mater. Struct.*, **33**(9), 093002. https://doi.org/10.1088/1361-665X/ad5809.

Zheng, Y.F., Qu, D.Y., Liu, L.C. and Chen, C.P. (2023), "Size-dependent nonlinear bending analysis of nonlocal magneto-electro-elastic laminated nanobeams resting on elastic foundation", *Int. J. Nonlin. Mech.*, **148**, 104255. https://doi.org/10.1016/j.ijnonlinmec.2022.104255.

Zou, X., Yan, G., Wu, W., Yang, W., Shi, W. and Sun, Y. (2023), "Effect of thickness stretching and multi-field loading on the results of sandwich piezoelectric/piezomagnetic MEMS", *Steel Compos. Struct.*, **46**(4), 485. https://doi.org/10.12989/scs.2023.46.4.485.

CC